Adv Polym Sci (2010) 227: 33–73
DOI:10.1007/12_2010_54

Published online: 25 March 2010

Nanopattern Evolution in Block Copolymer Films: Experiment, Simulations and Challenges

Larisa Tsarkova, G.J. Agur Sevink, and Georg Krausch

Abstract The present contribution reviews novel insights into block copolymer phase behavior and nanostructure formation in confined geometries. We focus on state-of-the-art experimental and theoretical progress in this area, with an emphasis on characterization methods and techniques that provide a quantitative framework for fundamental analysis. We discuss and compare basic system parameters that are readily controlled in simulations and in experiments, and present comparative studies of increasing degree of complexity concerning the phase behavior and ordering dynamics of cylinder- and lamella-forming block copolymers in thin films.

Keywords Nanostructures · Block copolymers · Thin films · Computer simulations · Scanning force microscopy

Contents

L. Tsarkova (✉)
Universität Bayreuth, Physikalische Chemie II, 95440 Bayreuth, Germany
e-mail: larisa.tsarkova@uni-bayreuth.de

G.J.A. Sevink
Leiden University, Leiden Institute of Chemistry, PO Box 9502, 2300 RA Leiden, The Netherlands
e-mail: a.sevink@chem.leidenuniv.nl

G. Krausch
Johannes Gutenberg Universität Mainz, Mainz
e-mail: krausch@uni-mainz.de

Abbreviations

a_0	Bulk domain spacing
BCC	Body-centered cubic
$C_{\parallel}$	Parallel-oriented cylinder
$C_{\perp}$	Perpendicular-oriented cylinder
DDFT	Dynamic density functional theory
DSCFT	Dynamic self-consistent field theory
GISAXS	Grazing incidence small angle X-ray scattering
h	Film thickness
L	Lamella
MC	Monte Carlo
ODT	Order–disorder transition
P2VP	Poly(2-vinyl pyridine)
PB	Polybutadiene
PL	Hexagonally perforated lamella phase
PS	Polystyrene
SAXS	Small angle X-ray scattering
SB	Polystyrene-*block*-polybutadiene diblock copolymer
SBS	Polystyrene-*block*-polybutadiene triblock copolymer
SCFT	Self-consistent field theory
SCMF	Particle-based SCFT
SE	Spectroscopic ellipsometry
SFM	Scanning force microscopy
SV	Polystyrene-*block*-poly(2-vinyl pyridine) diblock copolymer
SVT	Polystyrene-*block*-poly(2-vinylpyridine)-*block*-poly(*tert*-butylmethacrylate) triblock copolymer
TEM	Transmission electron microscopy
ϕ	Polymer volume fraction

1 Introduction

Thin block copolymer films have been the subject of intensive research over the last few decades, using both experimental and theoretical means. This interest is primarily due to the high potential of block copolymers in (nano)technological applications (see [1–5] for comprehensive reviews) and stems from their intrinsic ability to phase-separate and (self-)assemble into uniform microdomains with tunable dimensions, as well as on the unlimited number of pathways for introducing nanostructure functionality. Applications of block copolymer thin films in nanotechnology range from masks for nanolithography [6, 7], templates for controlled arrangement of nanoparticles [8, 9] and fabrication of nanoporous films [10], photonic band-gap materials [3, 9], high-density information storage media [11, 12], and many other more intricate yet fascinating applications.

The recent success in control and optimization of block copolymer patterns as well as block copolymer-based hybrid structures has been enabled by significant advances in thin film modeling and characterization. In particular, the rather recent developments of realistic models and atomic imaging techniques has been key to the determination of fundamentals underlying structure formation and ordering in block-copolymer thin films [13–22]. Surface fields effects (i.e., modification of the interfacial interactions at the surfaces of the film) as well as constraints caused by the confinement (i.e., control over the substrate topography and/or film thickness) have proved to be effective in manipulating phase behavior (microphase separation and structure orientation) both at the film surface and in the interior of the film. Control of the above parameters is often referred to as the "bottom-up" approach, in order to emphasize the fundamental role of the confined geometry on structure formation.

Uniform orientation and long-range lateral order of the microdomains with low or even vanishing densities of defects are a prerequisite for applications in nanotechnology. The standard experimental routine, consisting of equilibration of block copolymers under elevated temperature or in a solvent vapor, has had limited success in this respect, despite considerable research efforts. Several alternative strategies utilizing external stimuli were developed to overcome this functional limitation of block copolymer patterns [19, 21, 23, 24]. Variation of the solvent quality and of the velocity of the solvent evaporation during preparation, for example, provide rather flexible means of controlling the resulting structures and their orientation relative to the film plane, but are prone to many undefined variables. Theoretical studies have guided experimentalists into the rationalization of microdomain ordering mechanisms upon application of external electric fields [25, 26], through utilization of graphoepitaxy (chemically or topographically patterned surfaces) [23, 27, 28], or by quenching thick films at temperatures close to the order–disorder transition (ODT) temperature [29].

The present paper focuses on recent progress in experimental, theoretical, and experimental-simulational comparative studies of nanostructure formation in confined geometries that have led to the disclosure of novel fundamental insights. We review in particular the detailed results for the phase behavior and ordering

dynamics in thin films of cylinder- and lamella-forming block copolymers. The emphasis lies on the characterization methods and techniques that provide quantitative information for analytical and simulational methodology. This new understanding is further used to analyze particular experimental conditions, which have to be varied in order to target specific applications of nanopatterns. Along with mapping phase behavior of swollen and molten block copolymers in thin films, we focus on issues that are seldom discussed in the literature: molecular architecture effects, including complex ABC terpolymers; collective defect dynamics; swelling under confinement; analysis of the microdomain dimensions and of structure in the interior of the films.

1.1 Block Copolymers

Block copolymers consist of two or more covalently bounded immiscible components (blocks) and belong to the class of ordered fluids that display crystal-like order on a mesoscopic length scale and fluid-like order at a microscopic scale. The mesoscopic structure formation in such systems is governed by competing interactions. The incompatibility of the monomers of different blocks provides the short range repulsion, which drives the phase segregation of the blocks into microdomains with mesoscopic length scales of 10–100 nm (microphase separation). A macroscopic phase separation is prohibited due to the covalent bond between the blocks.

In mean field theory, two parameters control the phase behavior of diblock copolymers: the volume fraction of the A block f_A, and the combined interaction parameter $\chi_{AB}N$, where χ_{AB} is the Flory–Huggins parameter that quantifies the interaction between the A and B monomers and N is the polymerization index [30]. The block copolymer composition determines the microphase morphology to a great extent. For example, comparable volume fractions of block copolymer components result in lamella structure. Increasing the degree of compositional asymmetry leads to the gyroid, cylindrical, and finally, spherical phases [31].

If there are no strong specific interactions between A and B monomers like hydrogen bonding or charges, the interaction parameter χ_{AB} is usually a positive value and is small compared to unity. Positive values of χ_{AB} indicate a net enthalpic repulsion of the monomers. If $\chi_{AB}N$ is large enough, the system minimizes the non-favorable contacts between A and B monomers by microphase separation (strong segregation). The induced order incorporates some loss of translational and configurational entropy. χ_{AB} is inversely proportional to the temperature of the system. Therefore, mixing of the blocks is typically enhanced at elevated temperatures. When the temperature of the system increases (χ_{AB} decreases), the entropic factors eventually dominate and the system becomes disordered. This process is called ODT. Since the enthalpic and entropic contributions scale as χ_{AB} and N^{-1}, respectively, the product $\chi_{AB}N$ controls the phase state of the polymer [31].

1.2 Physics of Block Copolymers in Thin Films

A block copolymer in a confined environment exhibits certain properties that can be characterized as thin film behavior. This behavior is primarily dictated by the enhanced role of surface/interfacial energetics, as well as by the interplay between the characteristic block copolymer spacings and the film thickness.

1.2.1 Surface Fields

Surface fields are defined as differences in the surface/interfacial energies between A and B blocks of the copolymer at the film surfaces. They determine to a great extent the film composition near the surfaces, i.e., the wetting conditions. The interfacial energetics and related wetting conditions for lamella-forming systems are explicitly delivered in the review by Fasolka et al. [32]. *Symmetric wetting* occurs when the same block is located at both interfaces. Alternatively, block copolymer films with different blocks at each surface, termed antisymmetric films in the case of lamella systems, exhibit *asymmetric wetting* conditions.

1.2.2 Surface Relief Structures

Preferential attraction of one of the blocks to the surface brakes the symmetry of the structure and results in layering of microdomains parallel to the surface plane through the entire film thickness. The energetically favored film thicknesses are then quantinized with the characteristic structure period in the bulk through the formation of surface relief structures, also called terrace formation. These structures were established initially for lamella systems [37–39] and later for cylinder- [40–43] and sphere-forming block copolymers.

Experimentally, nucleation and subsequent growth of surface relief structures have been investigated as a function of surface fields [44–46], molecular architecture [37], film thickness [39, 47, 48], and annealing conditions [37–40, 49]. A more detailed summary of the experimental studies can be found in recent reviews [15, 19, 50, 51]; theoretical work on this issue is summarized in [41, 42].

The spontaneous development of the macroscopic topographic features in spin-coated samples, or in samples prepared by a gradient combinatorial approach [52, 53], has been fruitfully used for the analysis of thickness-dependent morphological behavior by constructing phase diagrams of surface structures [43, 49, 53, 54].

An interesting, but little-exploited, strategy is to use a regular thickness gradient created by patterned substrates in order to achieve complex sequenced microphase-separated structures within macroscopic topographic patterns [55, 56].

1.2.3 Deviations from the Bulk Morphology

The intrinsic 3D interfacial curvature in compositionally asymmetric block copolymers provides extra degrees of freedom for the phase behavior in hexagonally structured microdomains. It is now well established that confinement of a cylinder-forming block copolymer to a thickness other than the characteristic structure dimension in bulk, together with surface fields, can cause the microstructure to deviate from that of the corresponding bulk material. Surface structures in Fig. 1 are examples of simulated [57–59] and experimentally observed morphologies [40, 49, 60–62] that are formed in thin films of bulk cylinder-forming block copolymers.

ABC terblock copolymers in confined geometries exhibit a higher versatility and complexity of phase behavior than do binary block copolymers, and this has only been partly explored so far [4, 18, 63].

With advanced knowledge of the underlying physics, the structure formation in block copolymer films can be guided to achieve the most desirable large-domain ordered surface patterns: striped patterns can be produced by aligning the lying cylinder phase or the up-standing lamella phase; dot-like patterns originate from the up-standing hexagonally ordered cylinders or body-centered cubic (BCC) sphere phases, as well as from the perforated lamella phase [21]. Complex gyroid structures have a narrow stability range, and are produced by ABC terblock copolymers [18].

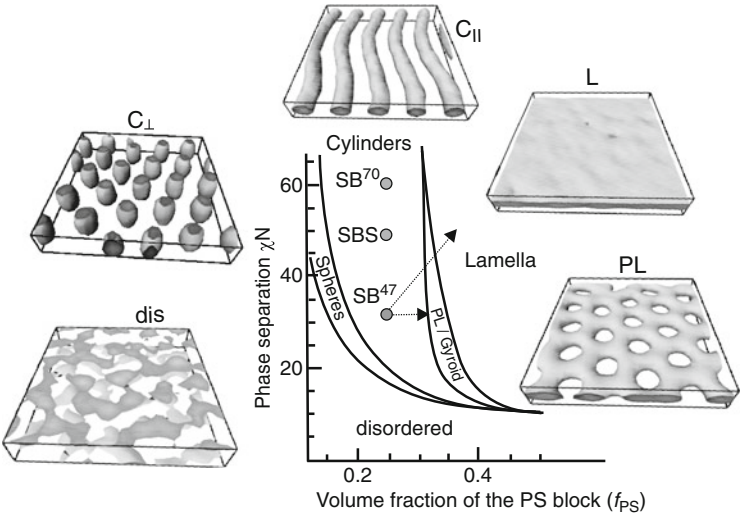

Fig. 1 Phase diagram of self-assembled structures in AB diblock copolymer melt, predicted by self-consistent mean field theory [31] and confirmed experimentally [33]. The MesoDyn simulations [34, 35] demonstrate morphologies that are predicted theoretically and observed experimentally in thin films of cylinder-forming block copolymers under surface fields or thickness constraints: *dis* disordered phase with no distinct morphology, $C_{\perp}$ perpendicular-oriented and $C_{\parallel}$ parallel-oriented cylinders, *L* lamella, *PS* polystyrene, *PL* hexagonally perforated lamella phase. *Dots* with related labels within the areal of the cylinder phase indicate the bulk parameters of the model AB and ABA block copolymers discussed in this work (Table 1). Reprinted from [36], with permission. Copyright 2008 American Chemical Society

2 Modeling with Computer Simulations

During the last two decades, block copolymer self-assembly in 1D confinement has been studied in great detail by a number of analytical and computational methods. In spite of the peculiarities of these methods (i.e., benefits and limitations), all of them apply some form of averaging over degrees of freedom in order to remain computationally tractable and all provide a coarse-grained description of phenomena in the mesoscopic regime (1–1000 nm). The purpose of this review is to list the fundamental insights obtained during a decade of collaboration between our computational and experimental groups using a very successful synergetic approach that enabled us to unravel several generic and essentially dynamical aspects of structure formation in cylinder-forming block copolymer thin films. It is not our intention to provide a complete overview of all theoretical efforts in this field or to give an extensive introduction into dynamic density functional theory (DDFT), the theory used in this review. For these aspects, the interested reader is referred to several existing reviews (e.g., [5, 15, 64]) and to the collected work on thin films of the Leiden group, in which the computational results are discussed in detail in relation to other experimental and theoretical findings. Here, we only briefly sketch the main directions in modeling structure formation in thin block copolymer films and emphasize the specific benefits of DDFT.

Before setting our modeling approach in context, we will focus on some general aspects of thin block copolymer film modeling. The majority of modeling studies so far have considered either coarse-grained particle-based Monte-Carlo (MC) computer simulations or field-based numerical calculations. Despite their relative success, a generic drawback of particle-based methods is that they, except in rare instances, are less capable of equilibrating sufficiently large systems of block polymers at realistic densities to extract meaningful information about structure and thermodynamics. For this reason, the parameter space in these studies is often rather limited. Few studies have used particle-based models that include a realistic kinetic description, e.g., dissipative particle dynamics (see, for instance, Kong et al. [65]).

Field-based models use a free energy that is either phenomenological or stems from an underlying coarse-grained molecular description, like in self-consistent field theory (SCFT) or DDFT [34, 35, 66]. These models overcome some of the drawbacks by further averaging and are clearly advantageous at melt densities and high molecular weights. The molecular field strategy in mean-field SCFT and DDFT involves a number of steps: (1) representation of the block copolymer by a suitable particle-based model, leading to a reduction of the degrees of freedom to particle coordinates; (2) conversion to a field theory by replacing the variables in the partition function from particle coordinates to one or more fluctuating potential fields; (3) discretization on a computational grid; and (4) sampling with the proper statistical weights.

A hybrid method, particle-based SCFT (SCMF) [67], was formulated as an alternative to mean-field SCFT and was applied to complex phenomena such as solvent evaporation in thin polymer films and reconstruction of chemically patterned substrates.

MC and mean-field SCFT were compared for thin films of lamellae-forming diblock copolymers [68]. The results showed an underestimation of the segregation of neutral solvent in SCFT and increasing discrepancy between SCFT and MC with decreasing chain length and temperature. The effect of composition fluctuations, which becomes particularly important for short chains and close to ODT, in lamellae-forming system has been studied using a field-theoretic approach that goes beyond the mean-field approximation [69] and particle-based simulations [70]. The influence of confinement close to ODT was also considered using alternative field models [71–73]. Other research directions used or adapted these methodologies to explore the effect of additional constraints, aimed at structure tailoring and defect-reduction, or optimized the (bulk) phase properties given desired thin film structures. Among the first directions were chemical linking of one block to the substrate [74] and chemical patterning of and/or introducing roughness to the confining surfaces [27, 45, 67, 75–86]. The second direction explores alternative molecular architectures, for instance ABC or dendrites, or mixtures of simple/cheap (di)block copolymers [6, 87–90]. The mechanical properties of such systems was also considered [91, 92].

In this review we describe on the theoretical results obtained for AB diblock or ABA triblock copolymer melts confined between two flat, homogeneous hard surfaces in the regime where fluctuations can be neglected (sufficiently long chains well below the ODT). Most studies in this field focused on the phase behavior of lamellae-forming symmetric diblock copolymers in confinement. Two general mechanisms were identified [13, 93–97]. For a commensurate film thickness (i.e., a film thickness that matches the discrete length scale set by the natural domain distances), the difference in surface-block interaction (the surface field) determines whether lamellae orient perpendicular (vanishing) or parallel (above a threshold) to the confining surface. Incommensurate film thicknesses give rise to stability of perpendicular lamellae. Confinement was therefore found only to affect the orientation of the (bulk) lamellar structure. In particular, mixed lamellar phases were found to be metastable by SCFT [13]. Only in the case of dissimilar block–surface interactions (i.e., different surface fields at each of the confining surfaces), were stable non-lamellar or hybrid structures identified in very thin films by SCFT [98]. Several studies considered defect dynamics and layer hopping in lamellae-forming systems [99–101].

Although these mechanisms are clearly general, the situation is considerably different for asymmetric AB or ABA block copolymers. First, confinement-induced chain deformations have been shown to lead to a stabilization of non-bulk morphologies in very thin films and parts of thicker films, even for similar interactions [62]. Second, microphase separation in these systems naturally gives rise to a matrix and a minority phase. Structure evolution and defect dynamics is clearly affected by these topological constraints and therefore very specific. The anticipated equivalence to lamella-forming systems is therefore partially lost. For these and other reasons, the thin film phase behavior of systems that form bicontinuous phases, cylinders, or spheres in bulk has attracted considerably less theoretical attention, despite their relevance in nanotechnology. Most studies on sphere-forming systems have focused

on packing of spherical domains in thin films, in particular on obtaining neat structures on a larger scale, and on the nature of the transition from a hexagonal structure in very thin (2D) films to the 3D (BCC) bulk lattice on increasing the film thickness [48, 102–106]. Only very recently were confinement-induced deviations from the bulk (sphere) structure studied using DDFT [107]. In cylinder-forming systems, our detailed DDFT studies for SB and SBS block copolymers are complemented by static phenomenological and mean-field SCFT calculations as well as by particle-based MC simulations (see [64, 97, 108–110]). In combination, they provide a complete and general picture of the fundamental phenomena, reviewed here, of cylinder-forming block copolymers in thin films.

The often-employed mean-field SCFT is a static theory, based on determining free energy minima or saddle points using mathematical techniques. SCFT is very well suited for determining equilibrium phase behavior (away from ODT). It is increasingly recognized, however, that experimentally accessed soft matter structures are often only metastable, even after very long equilibration, and that the understanding of dynamic pathways is therefore crucial for further development of soft matter material science. Although DDFT and SCFT share the free energy expression, the dynamic model in DDFT minimizes this free energy following collective diffusive dynamics, where the gradient of the chemical potential acts as a driving force. DDFT is therefore able to relate directly to the dynamic pathways and saddle points that are relevant in experimental systems, in a computationally efficient way. Despite the fact that some physical phenomena, like fluctuations, viscoelastic and hydrodynamic effects as well as chain entanglements, are not properly captured in this model, the work reviewed here shows that these contributions do not play a major role in these thin film systems. In addition, we note that the presence of neutral solvent in the experimental system was only considered as an effective scaling of the interaction parameters [62]. In particular, the (quasi)equilibrium and dynamic behavior was captured computationally in great detail (Sect. 4.5). We conclude that the theoretical approach provides a decisive understanding of the experimental results as it illustrates detailed microscopic mechanisms and allows for more extensive variations of the system parameters than one could achieve in experiments. Figure 2 compares the sample dimensions of the experiment with that of the computational simulation. In experiments, a typical film surface area available for the optical microscopy or scanning force microscopy (SFM) measurements is about a centimeter

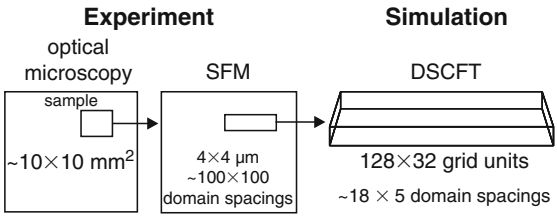

Fig. 2 Comparison of typical lateral scales that are covered in experimental measurements (optical microscopy and SFM) and in a simulation box. DSCFT is sometimes used as an acronym for DDFT. Reprinted from [41], with permission. Copyright 2007 American Chemical Society

square with an averaged terrace size of several micrometer square. Typically, in block copolymer films, each terrace accommodates in the lateral direction up to several hundred microdomains.

3 Characterization Techniques

The experimental studies on phase behavior and pattern formation reviewed here have been done on substrate-supported films of cylinder-forming polystyrene-*block*-polybutadiene diblock (SB) [36, 43, 51, 111–114] and triblock (SBS) [49, 62, 115–117] copolymers (Table 1), lamella-forming polystyrene-*block*-poly(2-vinyl pyridine) diblock copolymers (SV) [118, 119] and ABC block terpolymers of various compositions [53, 63, 120–131]. In simulation studies, a spring and bid model of ABA Gaussian chains has been used (see Sect. 2) [36, 42, 58, 59].

We present a brief summary of the original experimental approaches that allowed advances in the characterization and understanding of dynamic and equilibrium behavior on block copolymers under confinement.

3.1 Scanning Force Microscopy of Polymer Surfaces

The advent of advanced SFM methods facilitated surface studies of soft materials without causing damage to the sample. Typical problems in imaging polymeric samples with TappingMode concern the quantitative reproducibility of height and phase images, the distinction between real surface topography and indentation, and even the frequently occurring contrast inversion of height and phase images. These problems have been quantitatively addressed in [132]. In particular, the "real" surface topography can be distinguished quantitatively from the lateral differences in tip indentation. This approach allowed detection of a 10-nm-thick PB layer covering the true surface of SBS films [132].

Of particular importance are in situ SFM measurements, which allow real-time data collection during structure evolution [111, 112, 117, 133–135]. Both concentrated block copolymer solutions [117, 136, 137] and block copolymer melts [111, 112] have been imaged in situ to access the microdomain dynamics. Figure 3

Table 1 Copolymers of polystyrene and polybutadiene blocks

		Molecular weight		
Label	Structure	(kg/mol)	f_{PS} (wt%)	a_0 (nm)
SB^{47}	$S_{13}B_{34}$	47.3	26.1	30
SBS	$S_{14}B_{73}S_{15}$	102.0	26.0	40
SB^{70}	$S_{26}B_{70}$	96	24.5	64

f_{PS} refers to the fraction of PS in the copolymer, and a_0 to the bulk domain distance

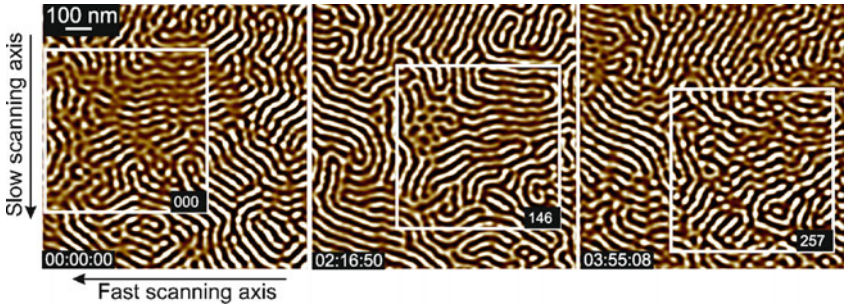

Fig. 3 Fourier filtered tapping mode SFM phase images of the surface structures in a fluid SB^{47} film at 105°C. The scale is 5° and bright corresponds to PS microdomains below an ≈10-nm-thick PB layer [132]. The images are frames from a SFM movie [111, 112] (the corresponding frame numbers and the elapsed time are shown). *White squares* highlight the same sample area that has been cut out for the movie. The *arrows* by the left image indicate the fast scanning axis, along which the tip moves with the velocity of 20 µm/s, and the slow scanning axis, along which the image is completed within ≈46 s. Reprinted from [111], with permission. Copyright 2006 American Chemical Society

shows the first frame, an intermediate frame, and the last frame from the sequence of continuously scanned SFM images. During the long term in situ measurements, the scanning area (highlighted by white squares) steadily moves due to thermal drift. We noted considerable changes to the surface structures with annealing time, making identification of the moving sample area of interest in snap-shot imaging experiments extremely difficult or even impossible. In Sect. 4.5 we describe original approaches towards the quantitative evaluation of dynamic SFM measurements [111, 112, 117, 136, 137].

Further challenge in SFM characterization of block copolymer structures is related to the precise measurements of the lateral dimensions. This analysis is possible when an SFM instrument meets the tight limits on axis orthogonality, flatness of the x,y plane, linearity, accuracy, and repeatability of the produced images. Recently, a home-built software has been used for the digital analysis of SFM Metrology images to evaluate confinement effects on the lateral dimensions of the microdomains [113]. Figure 4a presents a typical phase image of the cylinder structures aligned parallel to the film plane. Between two neighboring terraces, the film thickness increases gradually. The results of the analytical procedure are shown in Fig. 4b where characteristic distances between the cylinders are plotted as a function of the local thickness of the film (Sect. 4.4) [113, 138].

3.2 High Resolution Volume Imaging

Traditionally, SFM is limited to surface studies and sheds little light on the inner structure of the material. The nanotomography approach was suggested as a way

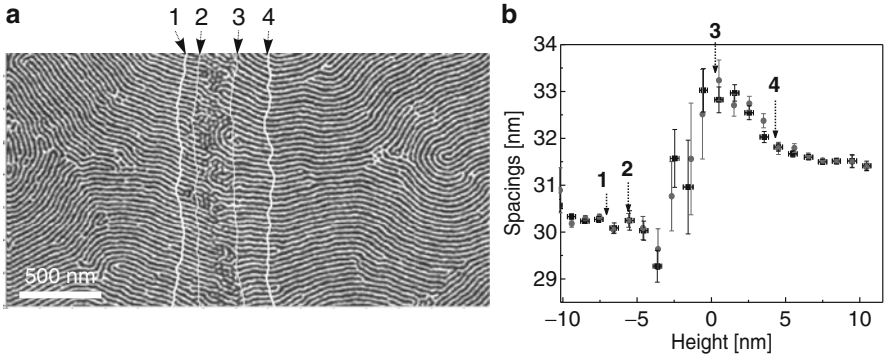

Fig. 4 (**a**) SFM phase image (3×1.5 μm) of the surface structures in SB^{47} films annealed in vacuum at 120°C. The *white contour lines* are taken from the height image (not shown) and mark the borders between the flat regions, as well as the transition region between the indicated terraces. (**b**) Spacings of cylindrical microdomains as a function of the local film thickness

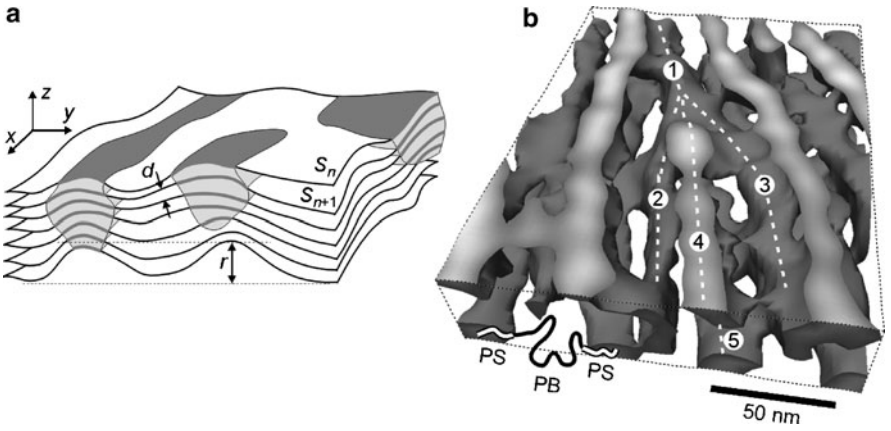

Fig. 5 (**a**) Illustration of the principle of volume reconstruction from a series of scanning probe microscopy images. (**b**) 3D image of the isosurface enclosing the volume with normalized TappingMode phase reconstructed from a series of phase and topography images. An SBS molecule bridging two PS cylindrical microdomains is sketched. Reprinted from [116], with permission. Copyright 2002 by the American Physical Society

to overcome the limitations of 2D imaging [115, 116, 139–141]. A key feature of nanotomography is that both the surface properties under study as well as the actual (and changing) shape of the surface are measured with SFM after each erosion step, and as a result a 3D nanostructure is reconstructed (Fig. 5).

The potential of the nanotomographic approach is supported by advances in automation of SFM imaging. State-of-the-art SFMs have general limits in performing harsh sample treatments because their design concept is focused on in situ scanning in a closed environment (liquid/heating cells). Aggressive treatments like plasma

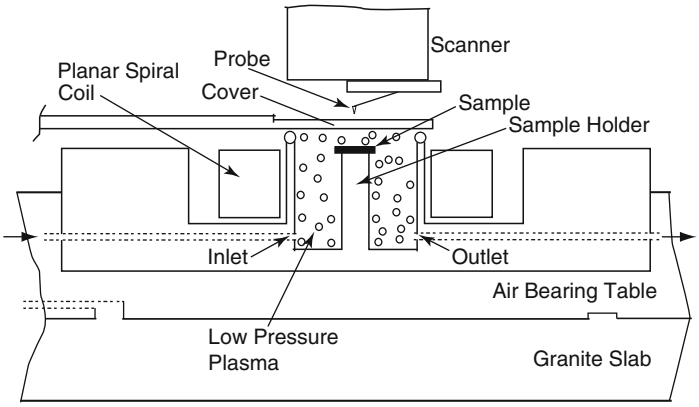

Fig. 6 Side view of the quasi in situ SFM prototype. The sample treatment and the scanning probe microscopic examination are temporally and spatially separated from each other. The probe is not affected by the sample treatment process, and a specific sample spot can be examined without readjustment. Reprinted from [142], with permission. Copyright 2007 American Institute of Physics

etching or etching in aggressive liquids typically require removing the sample from the microscope. Recently, a new SFM-based setup with quasi in situ sample treatment capability has been developed [142] (Fig. 6). Its capabilities have been demonstrated by successive plasma etching and imaging of lamella polymer films, which gives access to depth-profiling with high lateral and normal resolution [143]. The new development concerns the possibility of repositioning the SFM tip on a specific sample spot after successive treatments performed inside the SFM.

3.3 Annealing Under Controlled Conditions

Phase separation in block copolymer films has been shown to be sensitive to the solvent selectivity and its concentration in the film [49, 51, 114, 120, 123]. We emphasize the importance of a well-controlled atmosphere of solvent vapor for the annealing process since even slight changes in the solvent concentration or in the temperature of the system may induce structural phase transitions.

One of the easy and effective approaches for quantifying the polymer volume fraction within films in situ is to use in situ spectroscopic ellipsometry (SE) [49, 118, 119, 144]. The measurements should be performed in a thermostated cell (Fig. 7) with full control over the solvent vapor atmosphere p/p_0, where p_0 is the solvent vapor pressure at saturation and p is the actual pressure, which can be adjusted by a combination of the saturated vapor flow and dry nitrogen flow [118, 119], or by the difference between the temperature T_1 of the polymer sample and the temperature T_2 of the solvent vapor [49, 114, 144].

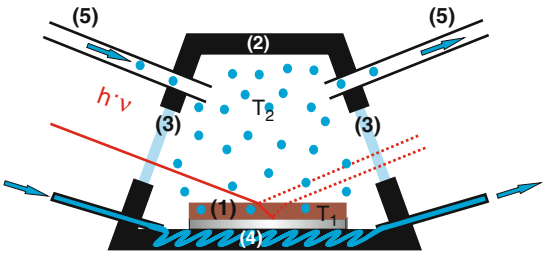

Fig. 7 Schematic of the annealing chamber: (1) substrate-supported polymer film; (2) sealed stainless steel chamber; (3) glass windows, which are perpendicular to the incident light; (4) temperature control of the substrate (T_1); (5) input and output for the temperature- and flow-controlled solvent vapor (T_2). Reprinted from [114], with permission. Copyright 2009 American Chemical Society

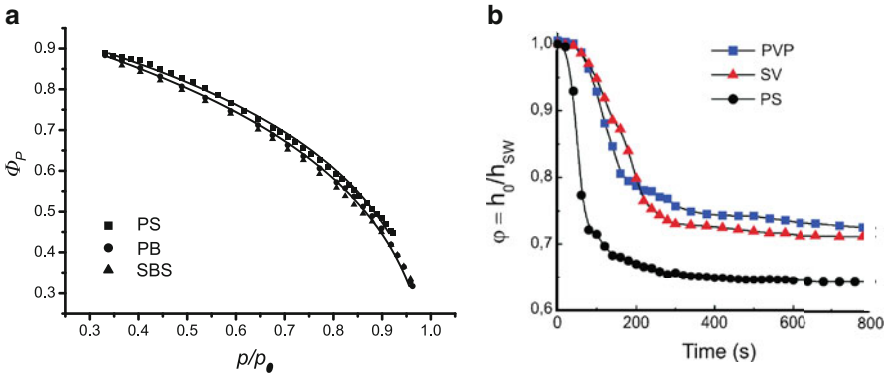

Fig. 8 Polymer volume fraction $\phi = h_0/h_{sw}$, where h_0 is the thickness of the polymer film after spin-coating and h_{sw} is the thickness of a swollen film, measured by in situ spectroscopic ellipsometry as a function of (**a**) the relative solvent vapor pressure for thin films of homopolymers PS, PB, and SBS block copolymer. Reprinted from [49], with permission. Copyright 2004 American Institute of Physics. (**b**) Polymer volume fraction as a function of the swelling time for PS-*b*-P2VP (SV) block copolymer and for homopolymers PS and P2VP at $p/p_0 = 1.0$ [118]. The equilibrium degree of swelling indicates that toluene is a selective solvent for the PS block, and that SV block copolymer shows asymmetric swelling under toluene vapor. Reproduced by permission of The Royal Society of Chemistry (RSC) [118]

Figure 8a displays ϕ_{pol} as a function of the relative chloroform vapor pressure p/p_0 in films of PS and PB homopolymers, and in films of SBS block copolymer [49]. It shows that chloroform is a good solvent for both homopolymers, exhibiting only a small selectivity to PB. Figure 8b displays kinetic measurements of the swelling behavior of a symmetric SV block copolymer and of respective homopolymers at controlled toluene vapor [118]. The comparison of the equilibrium degree of swelling suggests that toluene is a selective solvent for the PS block. Moreover, the swelling behavior of the symmetric SV block copolymer is dictated by the P2VP component. Thus, the relative affinity of a solvent towards the block copolymer components can be accessed by well-controlled swelling experiments [144].

4 Block Copolymer Self-Assembly Under Confinement

The presence of external selective surfaces and confinement, in particular to dimensions comparable with the characteristic structure size, can considerably alter the microphase separation and stabilize non-bulk morphologies. Confinement effects on the surface and bulk film structures have been systematically analyzed in elegant experiments by Knoll et al. [49, 62] on thin films of concentrated solutions of SBS in chloroform. DDFT-based calculations on cylinder-forming ABA chains revealed stunning agreement in the sequence of stabilized morphologies between the calculated and the measured phase diagrams [43, 49, 57, 58, 62, 145]. As an example, Fig. 9 shows a comparison of the experimental results (upper panel) and the calculations (lower panel) for a given strength of the surface field [62]. A rich morphological variety is observed as the film thickness increases from left to right: a featureless wetting layer for the smallest thickness; dot-like pattern of vertically oriented cylinders $C_{\perp}$; striped pattern of parallel-oriented cylinders $C_{\parallel}$; hexagonally perforated lamella phase (PL), etc. The phase transitions occur at well-defined film thicknesses, highlighted by white contour lines, which are calculated from the SFM height images and represent borders of equal film thickness.

These results represent solid evidence for a general mechanism governing the phase behavior at surfaces and in thin films of modulated phases: The interplay

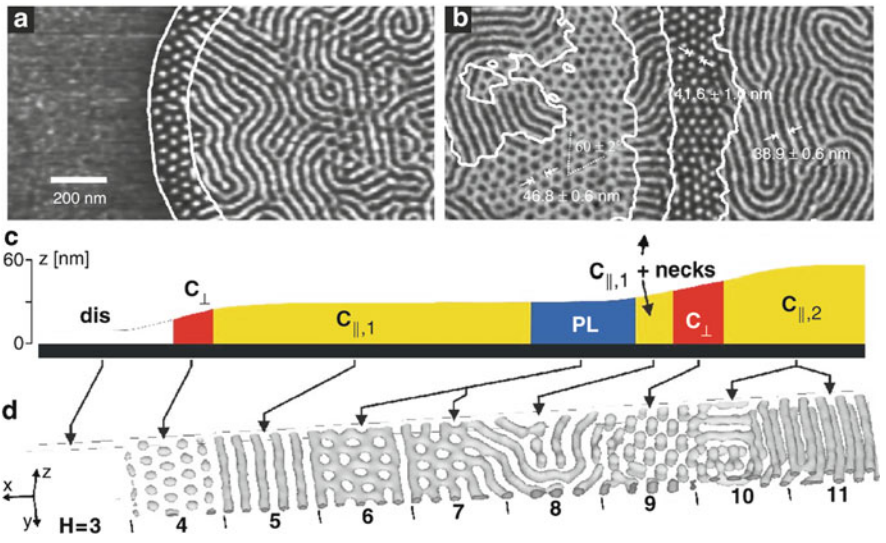

Fig. 9 (**a, b**) TappingMode SFM phase images of thin SBS films on Si substrates after annealing in chloroform vapor. The surface is covered with an approximately 10-nm-thick PB layer. *Bright* (*dark*) corresponds to PS (PB) microdomains in the top PB layer. *Contour lines* from the corresponding height images are superimposed. (**c**) Height profile of the thin film shown in (**a, b**). (**d**) Computer simulation of a block copolymer film in one large simulation box with increasing film thickness (from *left to right*). The isodensity surface of the density distribution of the A component ρ_A is shown for $\rho_A = 0$. Reprinted from [62], with permission. Copyright 2002 by the American Physical Society

between the strength of the surface field and the deformability of the bulk structure determines the system response, either via reorientation or via phase transitions and surface reconstructions. The stability regions of the different phases are modulated by the film thickness via interference and confinement effects.

4.1 Surface-Induced Phases in Melts

4.1.1 Simulations

We have used a slightly adapted version of the 3D DDFT implementation that was commercialized in the late nineties of last century as the MESODYN code. The adaptation was required to include asymmetric surface interactions. In general terms, all non-ideal chain interactions are included via a mean field and the strength of interaction between A and B components or blocks in the coarse-grained molecular chain representation is characterized by the interaction parameter ϵ_{AB}. This parameter is directly related to the conventional Flory-Huggins parameter χ and was determined based on a detailed mapping procedure [58]. Interfaces are treated as hard walls with reflecting boundary conditions, and proper constraints on the density. The interaction between chain components and interfaces (labeled by M) is characterized by corresponding mean field. As only the difference between the interactions of each component with the interfaces is relevant, we worked with effective interaction parameters $\epsilon_M = \epsilon_{AM} - \epsilon_{BM}$ which characterize the strength of each surface field. By setting $\epsilon_{BM} = 0$, a positive ϵ_M parameter corresponds to a repulsion between component A and the interface.

Variation of the preferential interaction of the block copolymer components with the substrate has proved to be an important tool for tuning the phase separation near the surfaces. The results of calculations in Fig. 10 quantify the effects of the surface fields in a solvent-free-cylinder-layer thick film. The variation of ϵ_{M} at constant

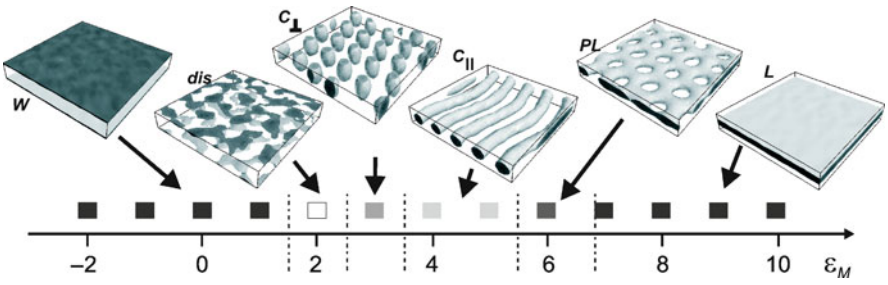

Fig. 10 Simulation results for a cylinder-forming $A_3B_{12}A_3$ ($\epsilon_{\mathrm{AB}} = 6.5$) in thin films (thickness $= 6nm = a_0$) with varied strength of the symmetric surface field ϵ_M. The isodensity profiles ($\rho_{\mathrm{A}} = 0.45$) are shown for indicated simulation parameters. Reprinted from [58], with permission. Copyright 2004 American Institute of Physics

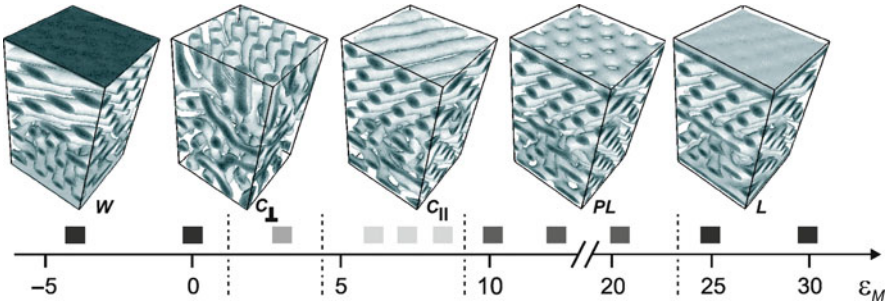

Fig. 11 Effect of the strength of the surface field ϵ_M on the phase separation in the interior of the film and at interfaces. Simulation results for a cylinder-forming $A_3B_{12}A_3$ ($\epsilon_{AB} = 6.5$) in thick films (thickness $= 54nm = 9a_0$) with surfaces at $z = 0$ and at indicated values of symmetric surface field ϵ_M. The isodensity profiles ($\rho_A = 0.45$) are shown for indicated simulation parameters. Reprinted from [58], with permission. Copyright 2004 American Institute of Physics [58]

film thickness induces structures ranging from the non-bulk lamella (at $\epsilon_M = 7$) and perforated lamella (at $\epsilon_M = 6$) to a disordered phase (at $\epsilon_M = 2$) with no well-defined microdomain structure, but with the two components A and B being still slightly segregated [58].

These and other results provide examples of an intriguing surface effect – deviations from the bulk microdomain structure in the vicinity of the interface – which has been called "surface reconstruction" owing to its analogy to the reconstruction in crystal surfaces. The effect is especially pronounced in films of relatively large thickness with nine microdomain layers ($h = 54$ nm) (Fig. 11). The main difference between the thin films of Fig. 10 and these thicker films is that in the vicinity of one film interface the influence of the other one is negligible. In the interior of the film in most cases the hexagonally ordered cylinders remain aligned parallel to the film plane. Depending on the strength of the surface field, considerable rearrangements of microdomains near the interfaces occur.

The calculated phase behavior for asymmetric surface fields, where the interactions between the components and the top (ϵ_{M1}) and bottom (ϵ_{M2}) interface may vary freely, is even much richer (see Fig. 12 for two layers of structure) than for the symmetric case. A particular feature is the appearance of hybrid structures, which are either a coexistence of different surface reconstructions close to each of the interfaces or interconnected structures. Nevertheless, the general features of Fig. 12 can still be explained in terms of surface field and confinement effects, noting that each of the surface fields now supports its own surface reconstruction, which may interconnect for combinations of perpendicular and parallel structures. As in the symmetric case, this behavior is modulated by the film thickness via interference and confinement effects in a very complicated manner.

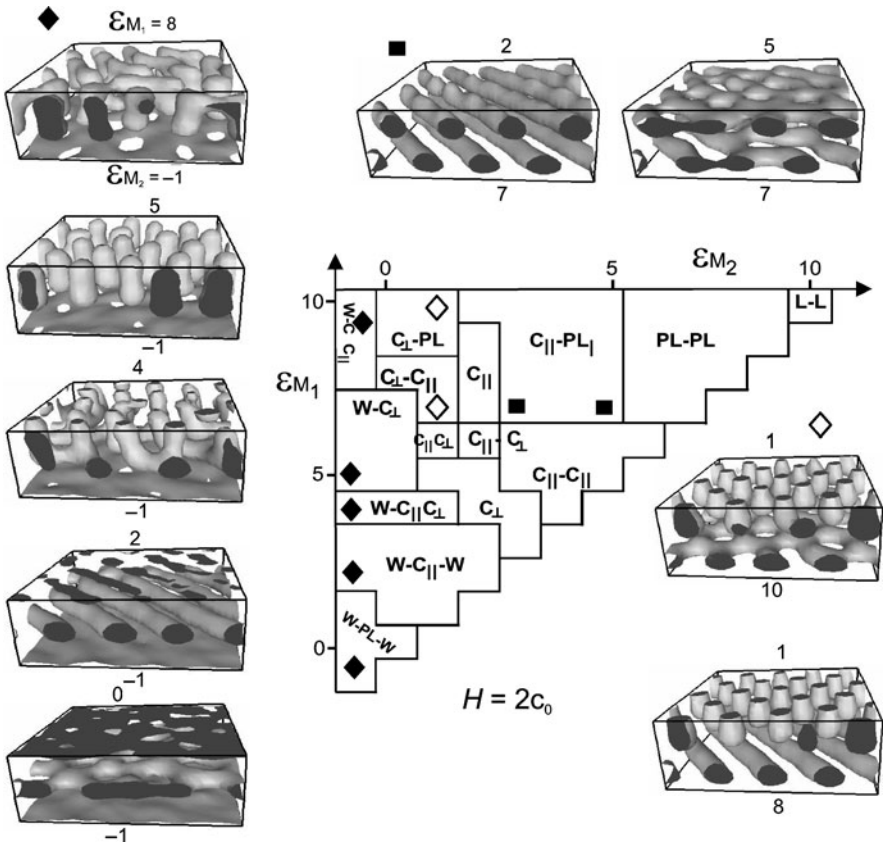

Fig. 12 Diagram of structures for varying interaction of the compounds with the top (ϵ_{M1}) and bottom (ϵ_{M2}) interface. *Symbols* denote the structures that are shown as *insets*. Isodensity profiles for $\rho_A = 0.45$ are shown, and the thickness h is twice the bulk domain distance a_0 (c_0 in [59]). Reprinted from [59], with permission. Copyright 2004 American Institute of Physics

4.1.2 Experiment

Various experimental routes towards surface modification have been utilized in order to control the microphase separation in thin films, as well as to achieve large-area patterns with desirable orientation relative to the film plane [2, 19, 21, 51].

In [43], the phase behavior and interlayer period of cylindrical domains have been tuned by varying the interactions with the substrate and by varying the related wetting conditions. Thin films of SB^{47} (Table 1) have been equilibrated by thermal annealing on two chemically different substrates and used as models of symmetric and asymmetric wetting. As seen from the experimentally established phase diagram in Fig. 13, on a neutral substrate (carbon-coated silicon) under asymmetric wetting conditions, cylinders are aligned parallel to the surface ($C_{||}$) both at the

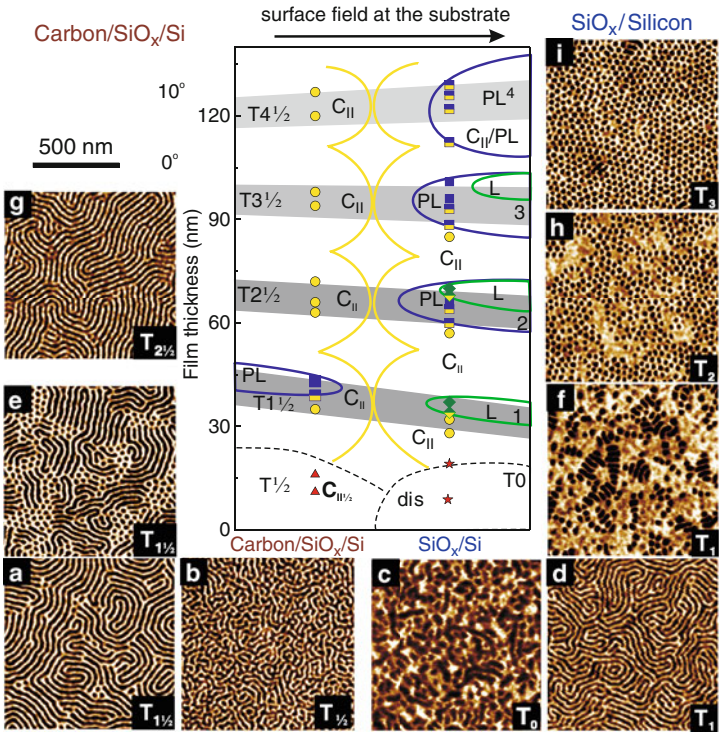

Fig. 13 Phase diagram of the surface structures on a weakly interacting surface (carbon coating) and under strong surface field with a preference for the majority component (silicon oxide). *Gray* areas mark the borders of the preferred film thickness (data taken from Fig. 14). The SFM phase images ($1 \times 1\,\mu m$) present examples of the surface structures on carbon-coated (*left*) and silicon oxide (*right*) substrates at the indicated film thickness. *Symbols* indicate the following morphologies: *circles* the $C_{\|}$ cylinder phase (**a**,**d**,**g**); *squares* the PL phase (**i**); *half-filled squares* coexisting $C_{\|}$/PL structures (**e**); *diamonds* the lamella (L) phase; *half-filled diamonds* coexisting $C_{\|}$/L patches (**f**) or coexisting PL/L microdomains (**h**); *triangles* half-cylinder structures $C_{1/2}$ (**b**); *stars* the disordered phase (**c**) [43]. *Black curves* schematically contour the phase boundaries and are drawn as a guide for the eye in line with the DDFT simulations [58]. Adopted from [43], with permission. Copyright 2006 American Chemical Society

favored (natural) and at the transition thicknesses. A half-cylinder phase $C_{1/2}$ forms in ultrathin films (with h below a_o, Fig. 13b) and probably also forms as a bottom layer in thicker films.

For a strong surface field and symmetric wetting conditions, a perforated lamella (PL) phase typically develops in up to four layers of structures, with an exception for the first layer of structures at the favored film thickness. For one layer and all transition regions between terraces a $C_{\|}$ phase was found.

The comparison of the surface structures on two substrates suggests strong surface effects on the microphase separation. For lamella systems, the degree of interfacial segregation has been shown to be proportional to the surface potential [146]. The same line of argument can be used to explain the surface field effects

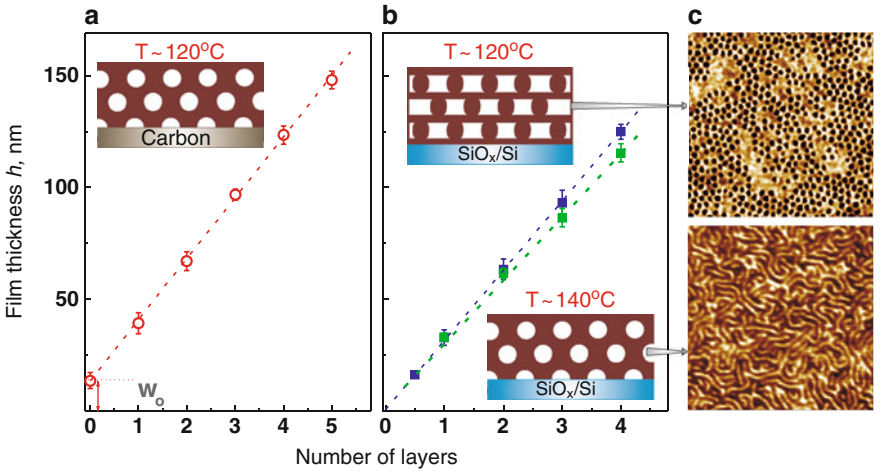

Fig. 14 Averaged terrace heights plotted versus the number of layers on (**a**) carbon-coated substrate (*circles*) at 120°C and on (**b**) silicon oxide substrate at 120°C (*blue squares*) and at 140°C (*green squares*). The *straight lines* are linear fits with the slopes corresponding to the mean interlayer distance: $c_{ca} = 27.4 \pm 0.2$ nm and $c_{si} = 31.1 \pm 0.2$ nm on the carbon-coated and silicon oxide substrates, respectively, at 120°C. The intercept on the carbon coating indicates a wetting layer of 13.4 ± 0.5 nm, which supports the upper layers. Increasing the annealing temperature to 140°C results in the phase transition from PL to the bulk cylinder morphology (**c**). The sketches introduce the tentative structure throughout the film and the related wetting conditions: symmetric wetting of the silicon substrate and the free surface by the PB (*dark*) component, and asymmetric wetting conditions on the carbon coating

in the cylinder phase: the strongly interacting silicon oxide surface affects the enthalpic interactions of the adsorbed monomers and thus increases the incompatibility of the block copolymer components, which in turn initiates phase transitions to non-bulk morphologies.

An important insight regarding the bottom-up assisted self-assembly of microdomains is provided by analysis of the equilibrium terrace heights. Figure 14 summarizes the effect of wetting and segregation conditions on the structure formation in block copolymer melts. The linear fits at 120°C for the two substrates differ in the slope and in the offset value at the thickness axis. We note that on increasing the annealing temperature to 140°C, the morphological transition to the bulk cylinder phase (SFM images in Fig. 14c) and the related decrease in the slope of the linear fit (Fig. 14b) were observed [138].

The interlayer period on the silicon substrate (Fig. 14b) strongly suggests that under a certain strength of the surface fields, the substrate-induced phase transition to non-bulk morphology propagates through the entire film thickness (in contrast to the simulation results in Fig. 11). Direct experimental evidence on the propagation range of the surface-induced reconstructions can be provided by in-depth profiling of block copolymer materials (see Sect. 3.2). Here, we emphasize that recent success in utilizing chemically and topogaphically patterned substrates confirms the efficiency of the bottom-up self-assembly approach [2].

4.2 Phase Diagrams of Surface Structures in Swollen Films

The equilibration of block copolymer films by exposure to solvent vapor is an alternative to the thermal annealing procedure. The resulting structures are extremely sensitive to the solvent evaporation rate [147–150] and exhibit structural polymorphism in the presence of selective solvents [122, 150–157]. Solvent-assisted fabrication of non-equilibrium highly ordered block copolymer patterns is a rapidly developing experimental approach that is very promising in terms of fundamental understanding and practical applications. Here, we focus on the equilibrium behavior of block copolymer films swollen with a non-selective solvent [49, 51]. A non-selective solvent in a swollen film acts as a plasticizer and effectively lowers the glass-transition temperature of the glassy components. As a result, the chain mobility is considerably enhanced without a significant increase in the processing temperature.

As established by Knoll et al. [49, 62], exposing thin films to well-controlled vapor pressure with a subsequent fast quench provides reproducible phase behavior under variation of the film thickness and of the polymer volume fraction (Fig. 15). At favored film thicknesses, cylinders orient parallel to the film plane, whereas a perpendicular orientation dominates at intermediate film thicknesses. In films thinner than 1.5 nm domain spacings and at high polymer concentration, the cylindrical

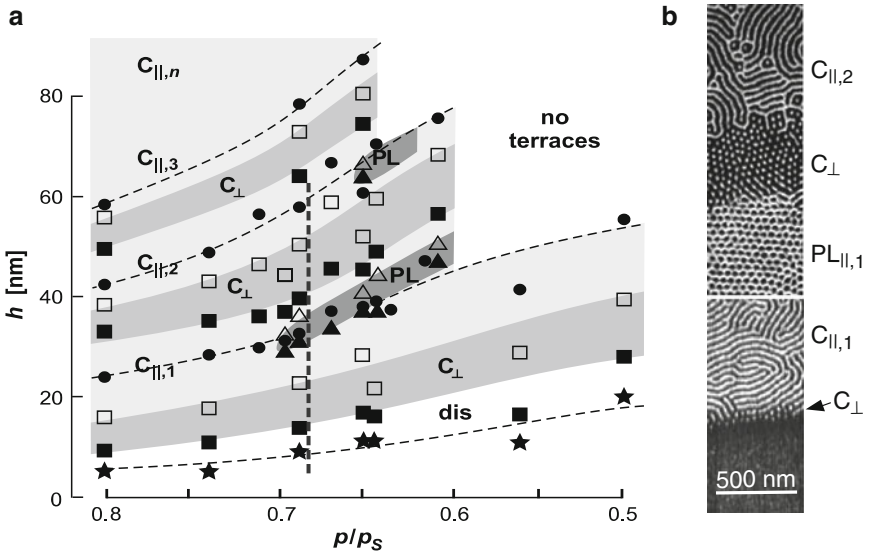

Fig. 15 (**a**) Phase diagram of the surface structures in SBS films (see Table 1) versus the partial chloroform vapor pressure. Horizontal *dashed lines* represent the energetically favored terrace thickness. Data are given for equilibrium film thickness of lying cylinders (*circles*), disordered structures (*stars*), and for upper and lower bounds (*open* and *closed symbols*, respectively) of upstanding cylinders (*squares*), and the perforated lamella phase (*triangles*). Reprinted from [62], with permission. Copyright 2002 by the American Physical Society. (**b**) Phase SFM images representing the indicated surface structures along the vertical *dashed line* in (**a**)

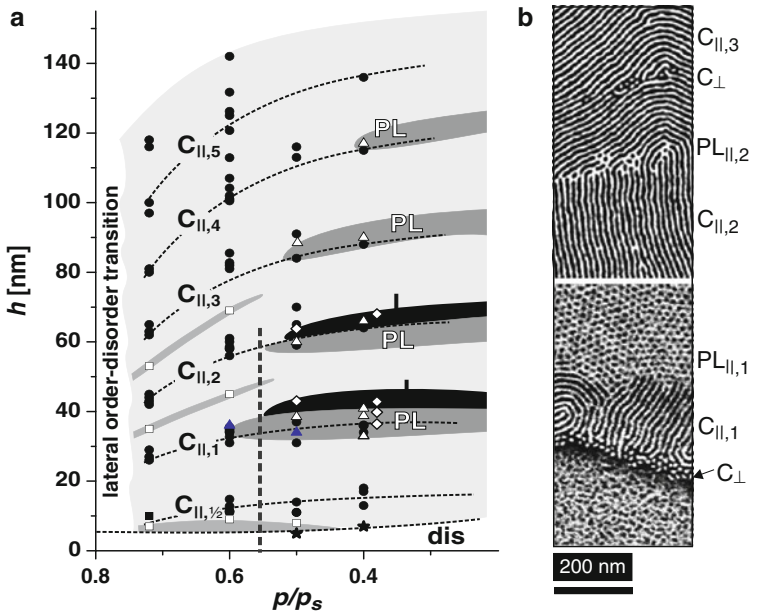

Fig. 16 (**a**) Phase diagram of the surface structures in SB^{47} films (see Table 1) versus the partial chloroform vapor pressure. Horizontal *dashed lines* represent the energetically favored thickness of the terraces. Data are given for equilibrium film thickness of lying cylinders (*circles*), disordered structures (*stars*), up-standing cylinders (*squares*), the perforated lamella (*triangles*), and lamella (*diamonds*) phases. (**b**) Phase SFM images representing the indicated surface structures along the vertical *dashed line* in (**a**)

microdomains reconstruct to the PL structure. These experimental results are in excellent agreement with model calculations based on the DDFT [58, 59, 62]. We have used the same experimental approach to study concentrated solutions of SB^{47} diblock copolymer in thin films. A comparison of the phase diagrams of surface structures in Figs. 15 and 16 suggests that the general phase behavior of SBS triblock copolymer is very similar to that of SB^{47} diblock copolymer. In particular, the same sequence of structures with increasing film thickness is observed (Figs. 15b and 16b), including deviations from the bulk structure, such as the PL and a wetting layer in ultrathin films. This confirms the universality of the reported phenomena. However, the phase diagrams differ in details, such as the position of the phase boundaries, the structure of the steps between the terraces, and the stabilization of the lamella phase and of vertically oriented cylinders. The established difference is presumably the consequence of the molecular architecture effects, which originate from the larger molecular weight of the middle majority block and from the possible loops- versus-tails chain arrangement in the microphase domains of ABA triblock copolymers. We note that in a recent theoretical study on the phase behavior of sphere-forming di- and triblock copolymers, a stabilization of vertically oriented cylinder phase (a deviation from the bulk morphology) has been reported for ABA systems [107].

4.3 *Confinement Effects on the Microphase Separation and Polymer–Solvent Interactions in Swollen Films*

The current trend towards miniaturization of functional systems and devices has driven the study of confinement effects (finite film thickness and the nature of the binding interfaces) on the fundamental physical properties of soft materials. Rapid developments of novel sensor and lab-on-chip technologies, and of polymer-based stimuli-responsive materials, raise the question of changes in solvent–polymer interactions under confinement.

Both, organo- and water-soluble polymers have been subjected to studies of their swelling dynamics, the distribution of the solvent within thin films, and the diffusion of the solvent. Furthermore, the distribution of the electron density along the depth of dried films has been studied using different experimental techniques including SE [158], optical reflectometry, X-ray or neutron reflectivity [159, 160], grazing incidence small angle X-ray scattering (GISAXS) [161], quartz crystal microbalance [162], and other complementary techniques.

In contrast to swollen homopolymer films, only a limited number of studies on thin films of block copolymers have been reported in which the degree of the film swelling has been directly accessed. In situ SE has been used to evaluate the polymer–solvent interaction parameters [144], to construct phase diagrams of surface structures [49, 51], and to control the mechanism of lamella reorientation in thick swollen films [118, 163, 164]. Spectroscopic reflectometry combined with real-time GISAXS has been used to follow structural instabilities in swollen lamella films [165]. Recently, it was demonstrated that swelling of diblock copolymer films in organic selective and non-selective solvents follows the same physical behavior as in thin films of homopolymers [119].

Up to now, published results contain non-consistent or even contradicting information concerning the influence of confinement on solvent absorption and distribution in a swollen film. In particular, the correlation between the absolute solvent uptake and the film thickness, as well as the effect of substrate interactions on the distribution of the solvent within the film, remain unclear. Here, we address solvent-assisted self-assembly of block copolymers, and present recent studies on the response of the microphase-separated patterns towards solvent uptake under controlled variation of the the film thickness, interfacial interactions, and of the solvent concentration in the atmosphere [114, 166]. This research brings novel insights into the degrees of freedom that govern self-assembly of soft matter in a confined geometry and indicates new approaches towards fabrication and functioning of nanostructured materials.

In our experiments, the quench from a swollen to a glassy state has been achieved within tens of seconds, and has been shown not to alter the phase separation in a swollen state[49]. Figure 17 compares surface structures in SB^{47} films that have been exposed to a relative vapor pressure p/p_0 of 72% and of 80%. With an increase of the solvent concentration, the in-plane order of the microdomains

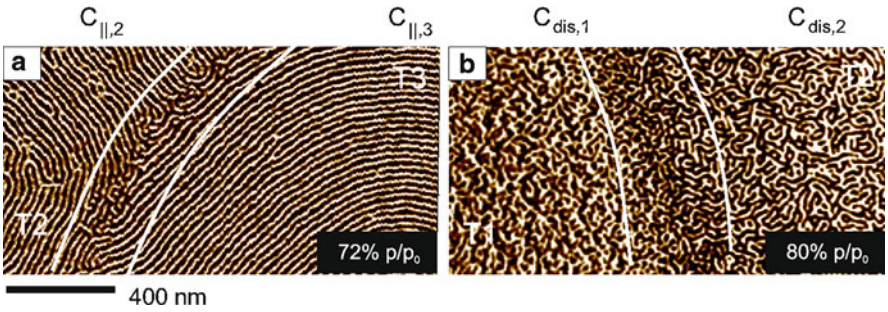

Fig. 17 SFM phase images (scale 10°) of SB^{47} films swollen with chlorofrom at (**a**) $p/p_0 = 72\%$ showing lying cylinders with a high degree of a long-range order, and (**b**) at $p/p_0 = 80\%$ showing a phase-separated pattern with a low long-range order (a disordered cylinder phase) [114]. White lines are guides for the eye and mark the borders of the areas with a constant film thickness

is dramatically reduced, indicating that the system is close to the ODT. In this segregation regime, the interface between two blocks is subjected to strong composition fluctuations [114, 166].

The increase of the solvent concentration in SB^{47} films on raising the partial pressure of chloroform vapor, and the related loss of long-range order, can be explained in terms of the so-called "dilution approximation" for the bulk block copolymer phases [167, 168]. The above results clearly demonstrate the high sensitivity of the polymer–polymer interactions towards solvent content. Therefore, the microphase-separated structures in swollen block copolymer films can be used as a qualitative measure of the degree of swelling of the films [49, 166].

Along with the surface interactions, the chain conformation that is imposed by the confined geometry and by the film preparation strongly affects the swelling behavior of polymer films [119, 169–171].

Figure 18a,b displays SFM images of SV films that have been prepared from chloroform and from toluene solutions, respectively. The mixed pattern of featureless areas and round-shaped stripes in Fig. 18a can be identified as in-plane lamella and perpendicular-oriented lamellae, respectively. The microstructure prepared from toluene solutions (Fig. 18b) is attributed to P2VP micelles surrounded by the PS shell. The micelle morphology is a result of the SV self-assembly in a selective solvent [119]. We have made use of this morphological difference to study the microstructure response to solvent uptake by block copolymer films.

Figure 18c displays swelling kinetics of two SV films with the same initial thickness but different microphase-separated structures. The curves show up to 10% larger swelling (smaller ϕ_{pol}) of SV films with the initial bulk lamella morphology as compared to the films with the non-bulk micelle phase [119].

This difference is probably associated with the chain expansion and/or contraction relative to the interface between the blocks within the particular morphology. In analogy to solid inorganic materials whose solubility increases under external pressure and to colloid systems where the capillary pressure leads to an increase in the solubility (Ostwald ripening effect), one would intuitively expect larger swelling of

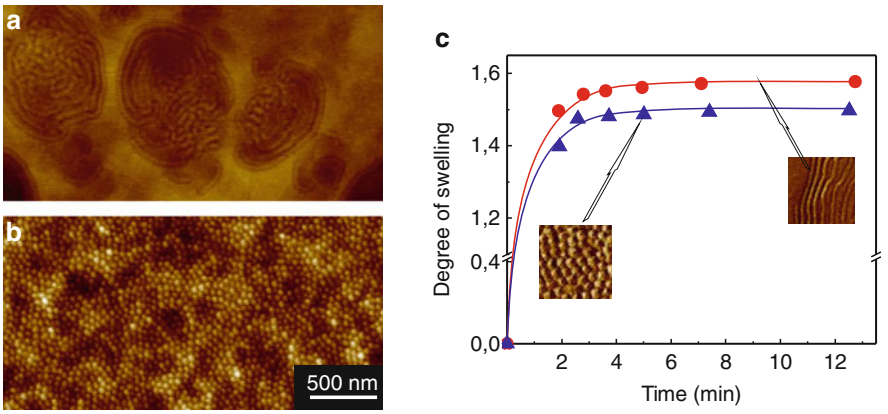

Fig. 18 SFM height images (scale 20 nm) of representative surface structures in SV films after spin-coating from chloroform solution (**a**), and from toluene solution (**b**). (**c**) Comparison of the swelling kinetics of ≈ 400-nm-thick SV films with starting micelle (*triangles*) and lamella (*circles*) morphologies

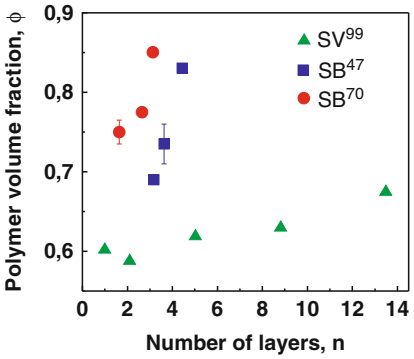

Fig. 19 Polymer volume fraction $\phi = h_{\mathrm{dry}}/h_{\mathrm{sw}}$ in swollen films of two PS-*b*-PB diblock copolymers (SB^{47} (*circles*) and SB^{70} (*squares*)) that have been equilibrated at $p/p_0 = 50\%$ of the partial chloroform (non-selective solvent) vapor pressure [114], and of SV films (*triangles*) equilibrated under $p/p_0 = 80\%$ of toluene (selective solvent) [119] versus the number of layers (film thickness normalized by the respective structure dimension in bulk)

the polymer chains that form non-bulk structures due to their stronger perturbation. However, we observed the opposite effect, which has to be considered in computer simulations and analytical theories on molecular conformations of block polymer chains in microdomain space.

Figure 19 summarizes the effect of confinement on the macroscopic swelling of the studied block copolymer systems. The systems differ in the molecular weight and composition of the studied block copolymers, in the solvent quality, and in the experimental conditions (which control the solvent atmosphere; see Sect. 3). At a constant vapor pressure, the equilibrium ϕ_{pol} for each polymer becomes smaller

as the film thickness decreases. The decrease of the solvent uptake by relatively thick SV film excludes a substantial contribution of an excess solvent layer at the polymer–substrate interface to an enhanced swelling of ultrathin films.

The established thickness-dependent degree of swelling discloses newly observed nanoscale effects of confinement on the chain conformations and on the polymer–solvent interactions in thin films. In particular, an easy and effective approach towards multilevel control over lamella orientation and order in thick diblock copolymer films has been demonstrated. The novel finding concerns the reorientation of lamella domains relative to the substrate upon equilibration under selective solvent [118]. The lamellar orientation perpendicular to the film plane on long-term selective solvent annealing was detected only in a narrow window of film thickness (between 19 and 22 characteristic lamella spacings in bulk L_0), and was confirmed by combined SFM, GISAXS, and TEM measurements (Fig. 20). Otherwise, lamellae were perfectly aligned parallel to the film plane due to surface field effects. The reorientation of lamella domains is attributed to the thickness-dependent degree of swelling when the concentration fluctuations in the interior of the film due to chain stretching overcome the suppression by the surface fields, which decline in strength

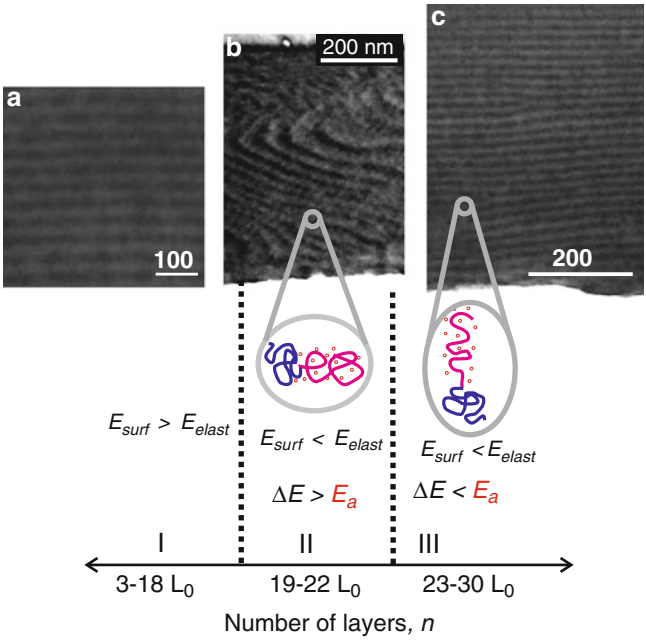

Fig. 20 Cross-sectional TEM images of equilibrated SV films within the respective thicknesses regions (**a**, **b**, **c**). The *dark regions* represent the stained P2VP microdomains. Schematic presents a qualitative analysis of the two contributions to the total free energy density of the system, E_{surf} and E_{elast}. E_{elast}. E_a is the activation energy for the reorientation of lying lamella to upstanding lamella [118]. L_0, lamella spacing in bulk. The sketches indicate that the chain conformation in regions II and III

with increasing distance from the boundary surfaces. We note that the combination of multiple fields based on solvent annealing and electric field yields an excellent control over the 3D orientation and order of lamellar microdomains [118].

4.4 Scaling of Cylinder Spacings in Thin Films

For an in-depth understanding of the self-assembly process in block copolymer films, a quantitative measure of the characteristic distances and their dependence on relevant physical parameters (temperature, chain length, etc.) is essential. In bulk, such measurements have typically been done by small angle X-ray scattering (SAXS) and the results are broadly in line with the theoretical predictions [172]. In thin films, however, the situation is considerably more difficult because conventional scattering experiments are barely possible due to the insufficient amount of material. In lamellar-forming block copolymers, neutron reflection experiments have successfully been used to determine the characteristic lamellar spacing in thin films [173, 174]. We present here quantitative experiments on characteristic lengths for compositionally asymmetrical block copolymers. The algorithm to quantify the characteristic lateral spacings in thin films of cylinder block copolymers is described in [113].

The results of the analytical procedure are shown in Fig. 21 where characteristic distances between the cylinders are plotted as a function of the local thickness of the film. Quite strikingly, we observed a systematic variation of the lateral spacing between the cylinders as the film thickness increases from n to $n+1$ layers of cylinders. Moreover, the characteristic spacings in the lower terrace was systematically

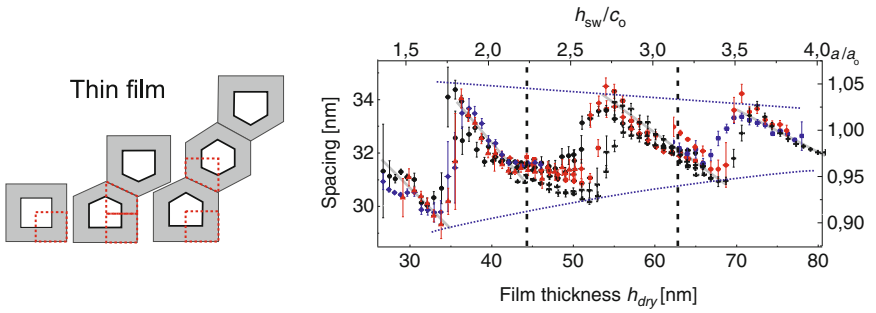

Fig. 21 Absolute microdomain spacings and reduced spacings versus the thickness h_{dry} of quenched films. Different symbols correspond to different measurements and experiments. The vertical *dashed lines* indicate the energetically favored film thicknesses at terraces. The straight *gray lines* emphasize different slopes of spacing relaxation on accommodation of the next layer of cylinders. Two *dotted lines* follow the minimum and maximum deviations of the macrodomain spacings from a_o, where a_o is the spacing in the bulk. (*Left*) Unit cells in thin films used for the strong-segregation theory calculation in [113]. The *dotted lines* denote the actual calculated geometries. Reprinted from [113], with permission. Copyright 2007 American Chemical Society

0.5–1 nm smaller than that in the neighboring higher terrace (Figs. 21 and 4). The differences in the lateral spacings in the adjacent terraces vanish in the fourth layer [113]. The effect is clearly measurable and points to 1D stretching of a unit cell in thin block copolymer films.

The digital spacing analysis and its applications present a novel type of quantitative characterization of thin structured films. In particular, changes to the cylinder spacings in thermally annealed films with the variation of the annealing temperature suggested stronger segregation under confinement relative to the bulk melt at the same temperature [51, 138]. Also, accumulation of spacings data during the development of a dewetting rim can be used for quantitative analysis of stress distribution within the moving front, which may bring insights into the rheological properties of polymer films on a mesoscale [51].

4.5 Microdomain Dynamics

The growing number of applications of nanopatterns in technology is a strong incentive to develop an improved understanding of ordering dynamics with the aim of controlling the resulting nanopatterned surfaces. The high degree of order relative to the film surfaces, as well as long-range in-plane order of the film, are imperative to applications of nanopatterned surfaces [2, 3, 19].

Common, though for many applications undesired, features in block copolymer nanostructures are point and line defects, grain boundaries, metastable phases, as well as distortions in microdomains orientation. The key role of the generation and annihilation of topological defects was emphasized in the studies on structural phase transitions, long range alignment, and reorientation of microdomains under shear and under electric fields. However, all these studies relied on indirect experimental evidence from scattering and other spatially averaging techniques.

In this section, we review our research on structural defects and their short- to long-term dynamics in block copolymer films using in situ SFM measurements at elevated temperatures, and DDFT-based simulations. The strength of our approach is that structures visualized with SFM 2D are directly compared with computational structures that provide access to the structure away from the surface of imaging, in the interior of the film. We focus on specific defects in the cylinder phase that are kinetically trapped in thermal equilibrium during the lateral ordering of lying microdomains. While topological defects in polymer thin films resemble those commonly observed in other forms of ordered matter, block copolymers exhibit morphological and dynamic properties that are specific to their polymeric nature [175–180].

4.5.1 Classification of Characteristic Defects

We distinguish between classical, modified, specific, and grain boundary defect configurations. Figure 22 presents examples of simulated and measured classical

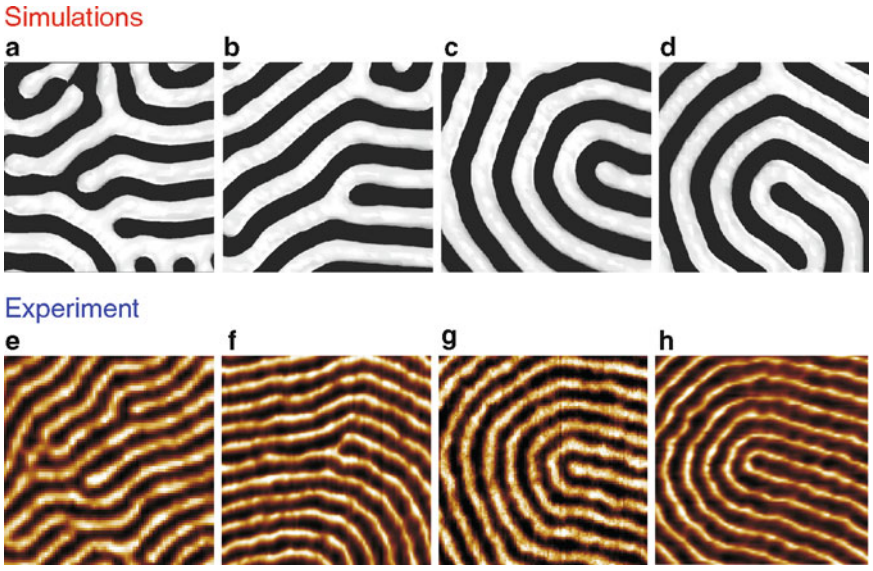

Fig. 22 Simulated images (*upper panel*) and SFM phase images (300×300 nm) (*lower panel*) presenting classical topological defect configurations in lying cylinders: (**a, e**) cyl-dislocation; (**b, f**) m-dislocation; (**c, g**) $+1/2$ cyl-disclination; and (**d, h**) $+1/2$ m-disclination. SB films were annealed under 70% of the saturated vapor pressure of chloroform. Reprinted from [36], with permission. Copyright 2008 American Chemical Society

defects in triblock and diblock copolymers. Purely topological arguments are sufficient to describe defects in films with upstanding lamella, since a topological defect always implies the abruption of one component. In contrast, in cylindrical phases the major dark-colored matrix (PB phase) is always interconnected, but the 2D representation of topological defects conceals this important property.

In order to account for the real 3D structure of cylindrical microdomains, we denote the configurations in Fig. 22a, e and c, g as cylinder-phase defects (cyl-dislocation and $+1/2$ cyl-disclination), and the configurations in Fig. 22b,f and d,h as matrix defects (m-dislocation and m-disclination). In our systems, cyl-dislocations generally develop during the early stages of film annealing when the overall defect density is high. In well-equilibrated films, cyl-dislocations are less frequent as compared to m-dislocations.

Modified Classical Defects

The rich phase behavior of cylinder-forming block copolymers is reflected in the modification of classical defects by incorporation of elements of non-bulk structures such as $+1/2$ disclination with incorporated PL ring (Fig. 23a, d) or white dot (b, e); and $-1/2$ disclination with incorporated PL domain (Fig. 23c, f). Defects Fig. 23a and b are topologically equivalent, but functionally different. Their

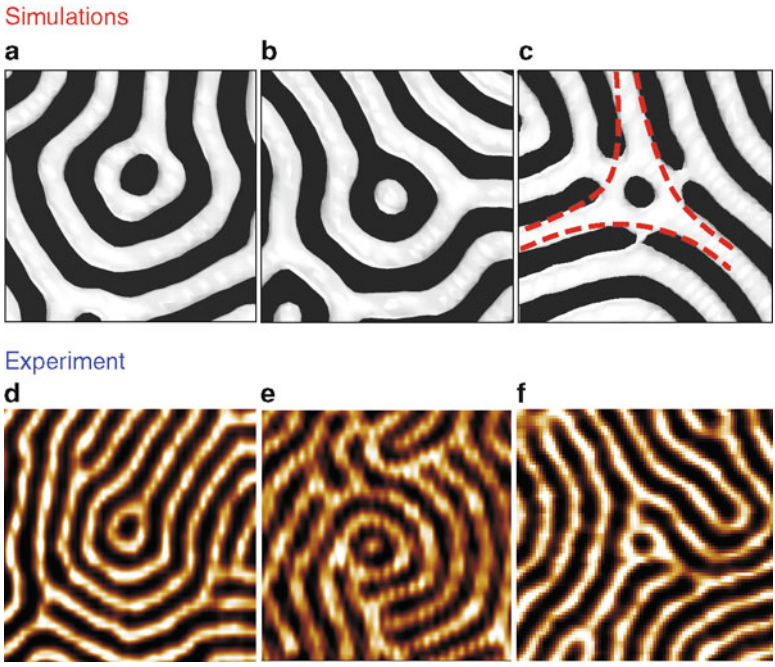

Fig. 23 Simulated images (*upper panel*) and SFM phase images (300×300 nm) (*lower panel*) presenting specific defect configurations: $+1/2$ disclination (**a, d**) and $-1/2$ disclination (**c, f**) with incorporated PL fragment; (**b, e**) $+1/2$ dot-disclination. SB films were annealed under 50% of the saturated vapor pressure of chloroform. Reprinted from [36], with permission. Copyright 2008 American Chemical Society

temporal stability and role in the overall structure evolution are discussed in detail in [36]. In particular, the PL phase lacks the axial symmetry; therefore it effectively compensates large disorientations of cylinder grains.

Specific Defects

Figure 24 presents specific neck defects, which can be viewed as a closely interacting pair of m-dislocations (Fig. 24a and related sketch). Such necks provide connectivity of the minority phase and thereby facilitate material transport without crossing the PS–PB interface. Interestingly, in DDFT simulations neck defects are not seen in the ordered cylinder phase. This fact probably indicates a small energy difference between the neck defect and the defect-free cylinders. Considering the experimental conditions when the necks between cylinders form, we conclude that their origin is driven by local concentration fluctuations.

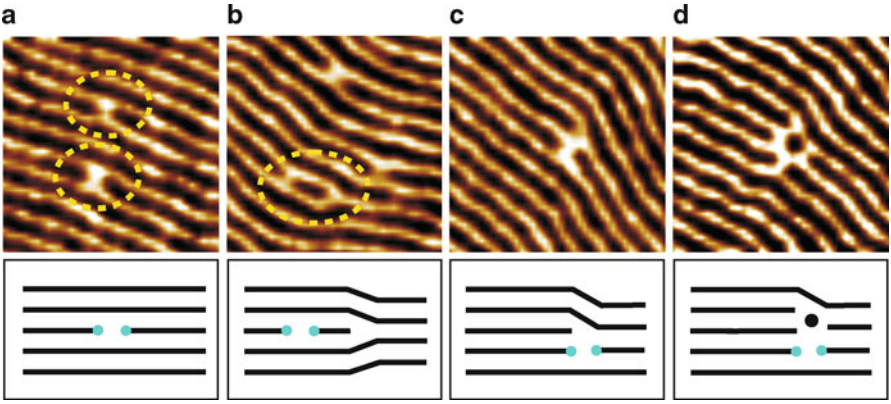

Fig. 24 SFM phase images of surface structures in SB films, which were equilibrated under 70% of the chloroform-saturated atmosphere, showing specific neck defects (**a**) highlighted by *dashed circles*; interaction of neck-defects with m-dislocations (**b, c**), and with a single PL ring (**d**). Reprinted from [36], with permission. Copyright 2008 American Chemical Society

Detailed analysis of defect configurations in the cylinder phase and of their evolution allowed us to conclude that representative defect configurations provide connectivity of the minority phase in the form of dislocations with a closed cylinder end or of classical disclinations with incorporated alternative, non-bulk structures with planar symmetry. Further, block copolymers show a strong correlation between the defect structure and chain mobility on both short- and long-term time scales.

We note that earlier research focused on the similarities of defect interaction and their motion in block copolymers and thermotropic nematics or smectics [181, 182]. Thermotropic liquid crystals, however, are one-component homogeneous systems and are characterized by a non-conserved orientational order parameter. In contrast, in block copolymers the local concentration difference between two components is essentially conserved. In this respect, the microphase-separated structures in block copolymers are anticipated to have close similarities to lyotropic systems, which are composed of a polar medium (water) and a non-polar medium (surfactant structure). The phases of the lyotropic systems (such as lamella, cylinder, or micellar phases) are determined by the surfactant concentration. Similarly to lyotropic phases, the morphology in block copolymers is ascertained by the volume fraction of the components and their interaction. Therefore, in lyotropic systems and in block copolymers, the dynamics and annihilation of structural defects require a change in the local concentration difference between components as well as a change in the orientational order. Consequently, if single defect transformations could be monitored in real time and space, block copolymers could be considered as suitable model systems for studying transport mechanisms and phase transitions in 2D fluid materials such as membranes [183], lyotropic liquid crystals [184], and microemulsions [185].

4.5.2 Phase Transitions and Defect Evolution in Dynamic SFM Measurements and DDFT Simulations

Using the calculational method based on DDFT, deviations from the cylinder bulk morphology have been identified as surface reconstructions [58, 62]. The constructed structure or phase diagrams allowed surface field and confinement effects to be distinguished [57–59, 107, 145, 186]. The comparative analysis of defect types and dynamics disclosed annihilation pathways via temporal phase transitions [36, 111]. Further, a quantitative analysis of defect motion led to an estimate of the interfacial energy between the cylinder and the PL phases [117]. A DDFT-based model was effectively used to simulate a block copolymer film with a free surface and to study the dynamics of terrace development [41, 42]. We showed how our computational method and an advanced dynamic SFM can be exploited in a synergetic fashion to extend the information about the elementary steps in structural transitions at the mesoscopic level. In particular, the experiments validate the dynamic DDFT method, and the DDFT calculations rationalize the characterization of the film surface in the interior of the film [187].

In situ dynamic measurements and DDFT simulations to non-bulk PL and lamella morphologies (Figs. 25 and 26) demonstrate that annihilation of topological

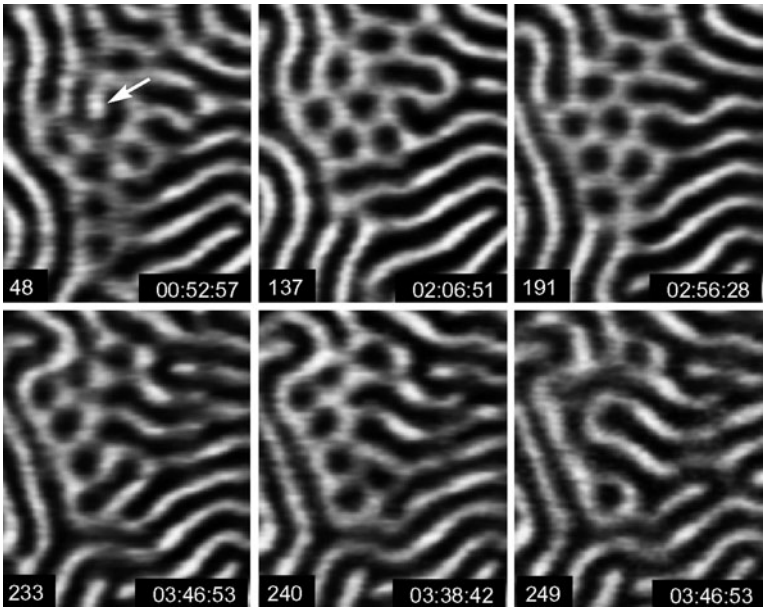

Fig. 25 SFM phase images showing the transient PL phase at the boundary between the cylinder grains. In *Frame 48*, an array of PL rings is aligned along the grain boundary and grouped around a "horse-shoe" defect (*arrow*). In *Frame 249* the transient phase is annihilated into the +1/2 disclination. The total evolution of the PL phase is about 4 h. The frame number and the elapsed time of the measurement are shown. Reprinted from [111], with permission. Copyright 2006 American Chemical Society

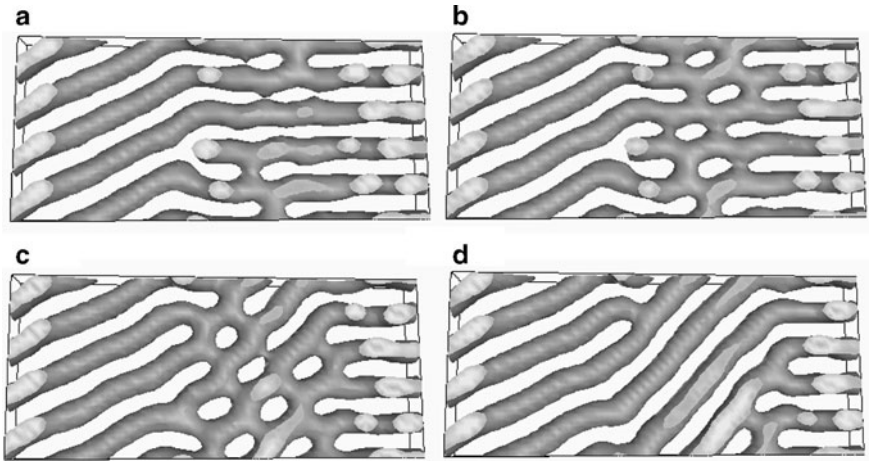

Fig. 26 Snapshots of DDFT calculations, modeling a thin supported film of $A_3B_{12}A_3$ cylinder-forming block copolymer in a $128 \times 32 \times 26$ bit volume. Crops of the middle layer, visualizing the reorientation of cylinders via the transient PL phase are shown after (**a**) 56,000, (**b**) 57,200, (**c**) 58,400, and (**d**) 59,600 time steps. The thin film morphology is shown by the isodensity surface of A component for a threshold value of $\epsilon_A = 0.33$. Reprinted from [111], with permission. Copyright 2006 American Chemical Society

defects in the cylinder phase in many instances proceeds via local temporal phase transitions. The low interfacial tension of $\sim 2.5\,\mu Nm^{-1}$ between the cylinder and the PL phases probably accounts for the energetically favorable pathway of structural rearrangements via phase transitions [117].

4.5.3 Evaluation of the Dynamic SFM Measurements

The high temporal resolution of SFM imaging uncovered elementary dynamic processes of structural rearrangements. We observed short-term interfacial undulations [111], fast repetitive transitions between distinct defect configurations [112], their spatio-temporal correlations on a length scale of several microdomains [112], and unexpected defect annihilation pathways via formation of temporal excited states [51, 111].

To analyze the temporal evolution of the microdomain oscillations between certain defect configurations, we associate the configurational energy of defects 1–2 and A–F in Fig. 27a with the number of open ends in the structures, and in Fig. 27b plot their temporal evolution. The thick gray curves highlight the periods of prevailing appearance of configurations with one open end and with two open ends. Within each of these periods there are short-time transitions into other configuration. The similarity of the averaging curves suggests that the events at the two neighboring sites are correlated on the scale of at least several domain spacings and

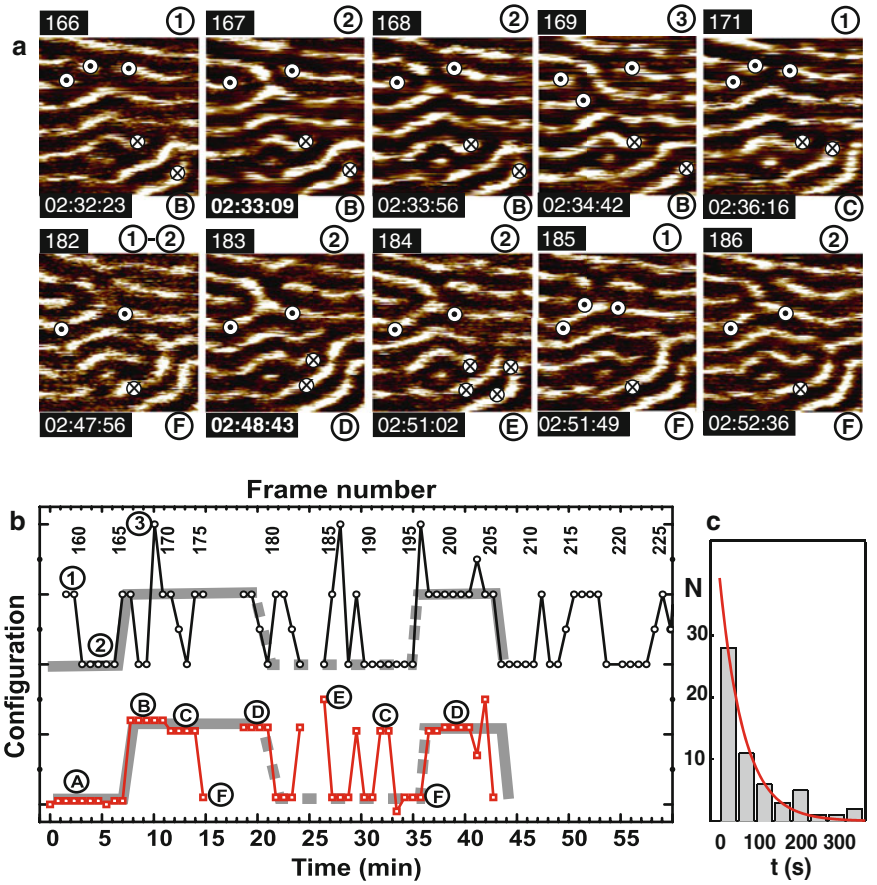

Fig. 27 (**a**) Crops (250 × 250 nm) from selected frames of the SFM movie showing the oscillations between distinct defect configurations. *Circled dot* and *crossed circle* mark the open ends of the cylinders. The structure marked with the *circled dot* fluctuates mainly between the configuration with three "open ends" (1) and the configuration with two "open ends" (2). The structure marked with the *crossed circle* fluctuates between configurations with one (*A*, *F*) or two "open ends" (*B*, *C*, *D*). (**b**) Temporal evolution of the defect configurations displayed in Fig. 27a. The configurations are sorted and grouped along the configuration coordinate according to their number of "open ends". The *gray curves* suggest correlations of defect dynamics. (**c**) Histogram of the time between two successive transitions shown in (**b**). Reproduced with permission from [112]. Copyright 2006 American Chemical Society

on a time scale of seconds. Moreover, we estimated the relaxation times involved and proposed possible molecular mechanisms that could account for these dynamics (Fig. 27c) [112]. Comparison of typical transition time with characteristic diffusion coefficients suggests that the motion proceeds via correlated movement of clusters of chains.

An original approach to the reduction and visualization of large sets of temporal evolution data has been recently presented [136]. Microdomains are reduced to thin smooth lines with colored branching points and visualized with a tool for protein visualization.

4.6 Structural Polymorphism of ABC Terpolymers

When a chemical variety of a linear block copolymer is increased to three different components, an intricate diversity of structures becomes possible [188, 189]. This is due to considerable increase in the number of involved polymer–polymer and polymer–surfaces interaction parameters. The studies on thin film behavior of ABC terpolymers are rare, even though they may potentially be more versatile than binary block copolymer morphologies due to the increased complexity.

Both theoretical [186, 190–192] and experimental [63, 123, 124, 128, 193] studies have demonstrated that interaction of the middle B block with a substrate plays a decisive role in the lamella structure orientation and order in thin films.

In the case of non-symmetrical volume composition, Elbs et al. facilitated different phases in polystyrene-*block*-poly(2-vinylpyridine)-*block*-poly(*tert*-butylmethacrylate) (SVT) films by exposing them to different solvent vapors (Fig. 28). Further studies indicated a large morphology dependence on the annealing vapor and drying conditions [4]. Rehse et al. demonstrated the presence of

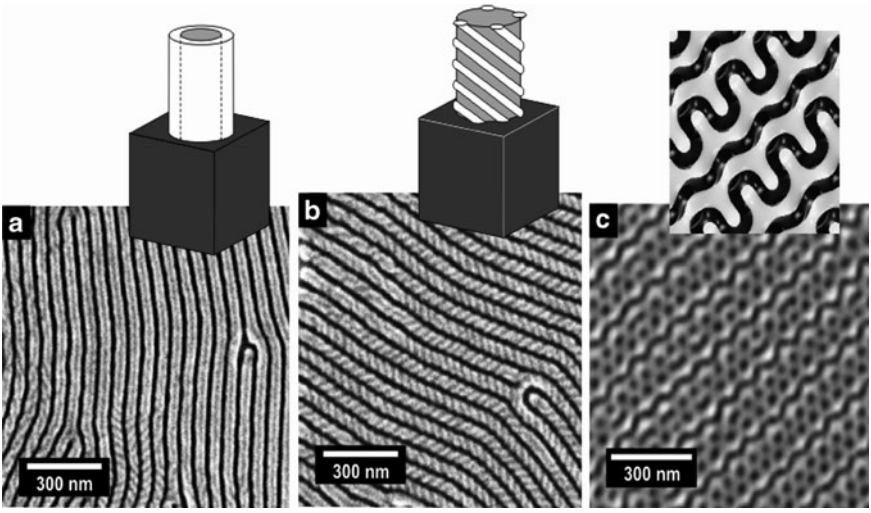

Fig. 28 SEM images of about 60 nm thick films of SVT block terpolymers along with expected structural elements of the thin-film structure. (**a**) Core–shell cylinders; (**b**) helices wound around a cylindrical core; (**c**) (112) plane of an ideal double gyroid structure. Copyright (2002) Wiley. Used with permission from [18]

non-bulk surface-reconstruction morphologies using ABC terpolymers of different compositions [126–128]. Ludwigs et al. systematically studied the phase behavior of SVT thin films [53, 63, 129, 130] and could match these results to DDFT calculations [186]. These studies demonstrated that confined systems are very sensitive to small changes in the energetic interaction between the different components, leading to a wide variety of possible surface reconstructed morphologies. Amongst other morphologies, a stable and highly ordered PL phase has been found, which could find use in membrane applications [63, 131]. The high order of the PL phase over macroscopically large areas was presumably caused by the bicontinuous nature of the morphology. Studies by other groups have been recently reviewed in [4].

5 Perspectives and Challenges

With advanced physical characterization techniques and theoretical analyses, the scientific understanding of the structure, dynamics, and thin film behavior of both compositionally simple and complex block copolymer architectures is rapidly expanding. The interest is supported, above all, by their growing importance in nanotechnology. The development is possible due to conjugation of new synthetic capabilities, processing methods, and self-assembly paradigms. Currently, attention is shifting towards new structural motifs for designing systems capable of hierarchical self-assembly into complex, well ordered, functional mesostructures.

Recent remarkable progress in polymerization techniques allows the preparation of well-defined tailor-made macromolecules, with precise control over the molecular weight, structure, architecture, and placement of functional groups [194]. A comprehensive review by Granick et al. [195] describes recommended synthetic directions and approaches, including the creation of organo-polymeric composites (light-emitting devices) and bio-related hybrid materials.

Increasing the structural complexity and functionality of new block copolymer materials while introducing additional hierarchy into self-assembly inevitably implies more complex dynamic routes for achieving the desired order on mesoscopic and macrososcopic scales. A detailed comparison between morphological studies and theoretical predictions will develop better understanding and control over the structure of functionalized block copolymers and will allow the tailoring of optical, mechanical, conducting, and other functional properties.

However, with the expanding spectrum of complexity and functionality of new polymer-based hybrid materials, no general routes and recipes for processing polymer-assisted materials should be expected. The effort to establish new approaches for guiding self-assembly of complex functional materials is the key to further technological application.

Acknowledgements This research has been supported by the DPG (Sonderforschungsbereich 481, TP B7/A9). The authors acknowledge the valuable contribution of R. Magerle, A.V. Zvelindovsky, A. Knoll, S. Ludwigs, A. Horvat, N. Rehse, H. Elbs, K. Lyakhova, J. Gensel, and M. Hund.

References

1. Park C, Yoon J, Thomas EL (2003) Polymer 44:6725
2. Li M, Coenjarts CA, Ober CK (2005) In: Abetz V (ed) Block copolymers II. Advances in polymer science, vol 190. Springer, Heidelberg, pp 183–226
3. Nie Z, Kumacheva E (2008) Nat Mater 7(4):277
4. van Zoelen W, ten Brinke G (2009) Soft Matter 5(8):1568
5. Hamley IW (2009) Prog Polym Sci 34(11):1161
6. Tang C, Lennon EM, Fredrickson GH, Kramer EJ, Hawker CJ (2008) Science 322(5900):429
7. Guo LJ (2007) Adv Mater 19(4):495
8. Haryono A, Binder WH (2006) Small 2(5):600
9. Hashimoto T, Fukunaga K (2007) In: Zvelindovsky AV (ed) Nanostructured soft matter: experiment, theory, simulation and perspectives. Springer, Heidelberg, pp 45–97
10. Hillmyer MA (2005) In: Block copolymers II. Advances in polymer science, vol 190. pp 137–181
11. Cheng JY, Ross CA, Chan VZH, Thomas EL, Lammertink RGH, Vancso GJ (2001) Adv Mater 13:1174
12. Thurn-Albrecht T, Schotter J, Kastle GA, Emley N, Shibauchi T, Krusin-Elbaum L, Guarini K, Black CT, Tuominen MT, Russell TP (2000) Science 290:2126
13. Matsen MW (1997) J Chem Phys 106:7781
14. Matsen MW (1998) Curr Opin Colloid Interface Sci 3:40
15. Fasolka MJ, Mayes AM (2001) Annu Rev Mater Res 31:323
16. Hamley IW (1998) The physics of block copolymers. Oxford University Press, Oxford
17. Hamley IW (2004) Developments in block copolymer science and technology. Wiley, Hoboken, pp 1–29
18. Krausch G, Magerle R (2002) Adv Mater 14:1579
19. Segalman RA (2005) Mater Sci Eng R Rep 48:191
20. Trawick M, Angelescu D, Chaikin P, Register R (2005) Nanolithography and patterning techniques in microelectronics. Woodhead Publishing, Cambridge, pp 1–38
21. Darling SB (2007) Prog Polym Sci 32:1152
22. Farrell RA, Fitzgerald TG, Borah D, Holmes JD, Morris MA (2009) Int J Mol Sci 10(9):3671
23. Cheng JY, Ross CA, Smith HI, Thomas EL (2006) Adv Mater 18:2505
24. Bita I, Yang JKW, Jung YS, Ross CA, Thomas EL, Berggren KK (2008) Science 321(5891):939
25. Böker A (2007) In: Zvelindovsky AV (ed) Nanostructured soft matter:experiment, theory, simulation and perspectives. Springer, Heidelberg, pp 199–229
26. Xu T, Wang J, Russel TP (2007) In: Zvelindovsky (ed) Nanostructured soft matter: experiment, theory, simulation and perspectives. Springer, Heidelberg, pp 171–198
27. Daoulas KC, Müller M, Stoykovich MP, Kang H, de Pablo JJ, Nealey PF (2008) Langmuir 24:1284
28. Ruiz R, Kang H, Detcheverry FA, Dobisz E, Kercher DS, Albrecht TR, de Pablo JJ, Nealey PF (2008) Science 321:936
29. Khanna V, Cochran EW, Hexemer A, Stein GE, Fredrickson GH, Kramer EJ, Li X, Wang J, Hahn SF (2006) Macromolecules 39(26):9346
30. Bates FS, Fredrickson GH (1990) Annu Rev Phys Chem 41:525
31. Matsen MW, Bates FS (1996) Macromolecules 29(4):1091
32. Fasolka MJ, Banerjee P, Mayes AM, Pickett G, Balazs AC (2000) Macromolecules 33:5702
33. Khandpur AK, Förster S, Bates FS, Hamley IW, Ryan AJ, Bras W, Almdal K, Mortensen K (1995) Macromolecules 28:8796
34. van Vlimmeren B, Maurits N, Zvelindovsky A, Sevink G, Fraaije J (1999) Macromolecules 32:646
35. Sevink GJA, Zvelindovsky AV, van Vlimmeren BAC, Maurits NM, Fraaije JGEM (1999) J Chem Phys 110(4):2250

36. Horvat A, Knoll A, Sevink GJA, Zvelindovsky AV, Krekhov A, Tsarkova L (2008) ACS Nano 2:1143
37. Liu Y, Zhao W, Zheng X, King A, Singh A, Rafailovich MH, Sokolov J, Dai KH, Kramer EJ (1994) Macromolecules 27:4000
38. Maaloum M, Ausserre D, Chatenay D, Coulon G, Gallot Y (1992) Phys Rev Lett 68:1575
39. Menelle A, Russell TP, Anastasiadis SH, Satija SK, Majkrzak CF (1992) Phys Rev Lett 68:67
40. Kim HC, Russell TP (2001) J Polym Sci B Polym Phys 39:663
41. Horvat A, Knoll A, Krausch G, Tsarkova L, Lyakhova KS, Sevink GJA, Zvelindovsky AV, Magerle R (2007) Macromolecules 40:6930
42. Lyakhova KS, Horvat A, Zvelindovsky AV, Sevink GJA (2006) Langmuir 22:5848
43. Tsarkova L, Knoll A, Krausch G, Magerle R (2006) Macromolecules 39:3608
44. Peters RD, Yang XM, Nealey PF (2002) Macromolecules 35:1822
45. Heier J, Kramer EJ, Groenewold J, Fredrickson GH (2000) Macromolecules 33:6060
46. Heier J, Sivaniah E, Kramer EJ (1999) Macromolecules 32:9007
47. Carvalho BL, Thomas EL (1994) Phys Rev Lett 73:3321
48. Yokoyama H, Mates TE, Kramer EJ (2000) Macromolecules 33:1888
49. Knoll A, Magerle R, Krausch G (2004) J Chem Phys 120:1105
50. Green PF, Limary R (2001) Adv Colloid Interface Sci 94:53
51. Tsarkova L (2007) In: Zvelindovsky AV (ed) Nanostructured soft matter:experiment, theory, simulation and perspectives. Springer, Heidelberg, pp 231–266
52. Smith AP, Douglas JF, Meredith JC, Amis EJ, Karim A (2001) Phys Rev Lett 87:015503
53. Ludwigs S, Schmidt K, Stafford CM, Amis EJ, Fasolka MJ, Karim A, Magerle R, Krausch G (2005) Macromolecules 38:1850
54. van Zoelen W, Polushkin E, ten Brinke G (2008) Macromolecules 41(2):8807
55. Bosworth JK, Black CT, Obert CK (2009) ACS Nano 3(7):1761
56. Park SM, Berry BC, Dobisz E, Kim HC (2009) Soft Matter 5:957
57. Huinink HP, van Dijk MA, Brokken-Zijp JCM, Sevink GJA (2001) Macromolecules 34:5325
58. Horvat A, Lyakhova KS, Sevink GJA, Zvelindovsky AV, Magerle R (2004) J Chem Phys 120:1117
59. Lyakhova KS, Sevink GJA, Zvelindovsky AV, Horvat A, Magerle R (2004) J Chem Phys 120:1127
60. Henkee CS, Thomas EL, Fetters LJ (1988) J Mater Sci 23:1685
61. Radzilowski LH, Carvalho BL, Thomas EL (1996) J Polym Sci B 34:3081
62. Knoll A, Horvat A, Lyakhova KS, Krausch G, Sevink GJA, Zvelindovsky AV, Magerle R (2002) Phys Rev Lett 89:035501/1
63. Ludwigs S, Böker A, Voronov A, Rehse N, Magerle R, Krausch G (2003) Nat Mater 2(11):744
64. Wang Q (2007) In: Zvelindovsky AV (ed) Nanostructured soft matter: experiment, theory, simulation and perspectives. Springer, Heidelberg, pp 498–528
65. Kong Y, Manke CW, Madden W, Schlijper A (1994) Int J Thermophys 15:1093
66. Fredrickson GH, Ganesan V, Drolet F (2002) Macromolecules 35:16
67. Daoulas KC, Müller M, de Pablo JJ, Nealey PF, Smith G (2006) Soft Matter 2:573
68. Wang Q, Nealey PF, de Pablo JJ (2002) Macromolecules 35:9563
69. Alexander-Katz A, Fredrickson G (2007) Macromolecules 40:4075
70. Nie Z, Su Z, Sun Z, Shi T, An L (2005) Macromol Theory Simul 14(8):463
71. Milner S, Morse D (1996) Phys Rev E 54:3793
72. Miao B, Yan D, Han C, Shi AC (2006) J Chem Phys 124:144902
73. Tsori Y, Andelman D (2001) Eur Phys J E 5(5):605
74. Matsen MW, Griffiths G (2009) Eur Phys J E 29:219
75. Nath SK, Nealey PF, de Pablo JJ (1999) J Chem Phys 110(15):7483
76. Tsori Y, Andelman D (2001) Macromolecules 34:2719
77. Tsori Y, Andelman D (2001) Europhys Lett 53:722
78. Tsori Y, Andelman D (2001) J Chem Phys 115:1970
79. Kim SO, Solak HH, Stoykovich MP, Ferrier NJ, de Pablo JJ, Nealey PF (2003) Nature 424:411

80. Tsori Y, Andelman D (2003) Macromolecules 36(22):8560
81. Tsori Y, Andelman D (2003) Interface Sci 11(2):259
82. Wang Q (2004) Macrom Theor Sim 14:96
83. Tsori Y, Sivaniah E, Andelman D, Hashimoto T (2005) Macromolecules 38:7193
84. Edwards EW, Stoykovich MP, Müller M, Solak HH, de Pablo JJ, Nealey PF (2005) J Polym Sci B 43:3444
85. Kim S, Kim BH, Meng D, Shin DO, Koo CM, Solak H, Wang Q (2007) Adv Mater 19:3271
86. Stoykovich M, Kang H, Daoulas KC, Liu G, Liu CC, de Pablo J., Müller M, Nealy PF (2007) ACS Nano 1:168
87. Koneripalli N, Levicky R, Bates FS, Matsen MW, Satija SK, Ankner J, Kaiser H (1998) Macromolecules 31(11):3498
88. Lee W, Elliott R, Mezzenga R, Fredrickson G (2009) Macromolecules 42:849
89. Hur SM, Garcia-Cervera C, Kramer E, Fredrickson G (2009) Macromolecules 42:5861
90. Tang C, Bang J, Stein G, Fredrickson GH, Hawker CJ, Kramer EJ, Sprung M, Wang J (2002) Macromolecules 35:9391
91. Ruokolainen J, Fredrickson GH, Kramer EJ, Ryu CY, Hahn SF, Magonov S (2002) Macromolecules 35:9391
92. Ryu CY, Ruokolainen J, Fredrickson GH, Kramer EJ, Hahn SF (2002) Macromolecules 35(6):2157
93. Pickett G, Balazs A (1997) Macromolecules 30:3097
94. Fasolka MJ, Harris DJ, Mayes AM (1997) Phys Rev Lett 79(16):3018
95. Geisinger T, Müller M, Binder K (1999) J Chem Phys 111(11):5241
96. Wang Q, Yan Q, Nealey PF, de Pablo JJ (2000) J Chem Phys 112(1):450
97. Meng D, Wang Q (2007) J Chem Phys 126:234902
98. Fasolka MJ, Banerjee P, Mayes AM, Pickett G, Balazs AC (2000) Macromolecules 33(15):5702
99. Tsori Y, Andelman D, Schick M (2000) Phys Rev E 61(3):2848
100. Boss A, Sides S, Katsov K, Garcia-Cervera C, Fredrickson G (2006) J Polym Sci B Polym Phys 44:2495
101. Croll A, Matsen M, Shi AC, Dalnoki-Veress K (2008) Eur Phys J E 27:407
102. Stein GE, Kramer EJ, Li X, Wang J (2007) Macromolecules 40:2453
103. Yokoyama H, Kramer EJ, Rafailovich MH, Sokolov J, Schwarz SA (1998) Macromolecules 31:8826
104. Segalman AR, Hexemer A, Kramer JE (2003) Phys Rev Lett 91(19):196101
105. Stein GE, Kramer EJ, Li X, Wang J (2007) Phys Rev Lett 98:086101
106. Stein GE, Cochran EW, Katsov K, Fredrickson GH, Kramer EJ, Li X, Wang J (2007) Phys Rev Lett 98:158302
107. Sevink GJA, Zvelindovsky AV (2009) Macromolecules. doi:10.1021/ma9014438
108. Wang Q, Nealey PF, de Pablo JJ (2001) Macromolecules 34(10):3458
109. Hammond MR, Sides SW, Fredrickson GH, Kramer EJ, Ruokolainen J, Hahn SF (2003) Macromolecules 36:8712
110. Khanna V, Cochran EW, Hexemer A, Stein GE, Fredrickson GH, Kramer EJ, Li X, Wang J, Hahn SF (2006) Macromolecules 39(26):9346
111. Tsarkova L, Horvat A, Krausch G, Sevink GIA, Zvelindovsky AV, Magerle R (2006) Langmuir 22:8089
112. Tsarkova L, Knoll A, Magerle R (2006) Nano Lett 6:2817
113. Knoll A, Tsarkova L, Krausch G (2007) Nano Lett 7:843
114. Zettl U, Knoll A, Tsarkova L (2009) Langmuir doi: 10.1021/la903922y
115. Konrad M, Knoll A, Krausch G, Magerle R (2000) Macromolecules 33:5518
116. Magerle R (2000) Phys Rev Lett 85(13):2749
117. Knoll A, Horvat A, Lyakhova KS, Krausch G, Sevink GJA, Zvelindovsky AV, Magerle R (2004) Nat Mater 3:886
118. Olszowka V, Tsarkova L, Böker A (2009) Soft Matter 5:812
119. Gensel J, Liedel C, Schoberth HG, Tsarkova L (2009) Soft Matter 5:2534

120. Elbs H, Fukunaga K, Stadler R, Sauer G, Magerle R, Krausch G (1999) Macromolecules 32(4):1204
121. Elbs H, Abetz V, Hadziioannou G, Drummer C, Krausch G (2001) Macromolecules 34(23):7917
122. Elbs H, Drummer C, Abetz V, Krausch G (2002) Macromolecules 35:5570
123. Fukunaga K, Elbs H, Magerle R, Krausch G (2000) Macromolecules 33(3):947
124. Fukunaga K, Hashimoto T, Elbs H, Krausch G (2002) Macromolecules 35(11):4406
125. Fukunaga K, Hashimoto T, Elbs H, Krausch G (2003) Macromolecules 36:2852
126. Rehse N, Knoll A, Magerle R, Krausch G (2001) Polym Mater Sci Eng 84:316
127. Rehse N, Knoll A, Konrad M, Magerle R, Krausch G (2001) Phys Rev Lett 87:035505
128. Rehse N, Knoll A, Magerle R, Krausch G (2003) Macromolecules 36(9):3261
129. Ludwigs S, Böker A, Abetz V, Müller AHE, Krausch G (2003) Polymer 44(22):6815
130. Ludwigs S, Schmidt K, Krausch G (2005) Macromolecules 38(6):2376
131. Sperschneider A, Schacher F, Gawenda M, Tsarkova L, Müeller AHE, Ulbricht M, Krausch G, Këhler J (2007) Small 3:1056
132. Knoll A, Magerle R, Krausch G (2001) Macromolecules 34:4159
133. Reiter G, Castelein G, Sommer JU, Röttele A, Thurn-Albrecht T (2001) Phys Rev Lett 87(22):226101
134. Yufa NA, Li J, Sibener SJ (2009) Macromolecules 42(7):2667
135. Hobbs JK, Mullin N, Weber CHM, Farrance OE, Vasilev C (2009) Mater Today 12(7–8):26
136. Scherdel S, Schoberth HG, Magerle R (2007) J Chem Phys 27(1):14903
137. Rehse S, Mecke K, Magerle R (2008) Phys Rev E 77:051805
138. Tsarkova, unpublished
139. Dietz C, Zerson M, Riesch C, Gigler AM, Stark RW, Rehse N, Magerle R (2008) Appl Phys Lett 92(14):143107
140. Rehse N, Marr S, Scherdel S, Magerle R (2005) Adv Mater 17(18):2203
141. Magerle R (2002) Lect Notes Phys 600:93
142. Hund M, Herold H (2007) Rev Sci Instrum 78(6):063703
143. Max E, Hund M, Tsarkova L (2008) PMSE Preprints 99:689–690
144. Elbs H, Krausch G (2004) Polymer 45(23):7935
145. Huinink HP, Brokken-Zijp JCM, van Dijk MA, Sevink GJA (2000) J Chem Phys 112:2452
146. Mansky P, Russell TP, Hawker CJ, Mays J, Cook DC, Satija SK (1997) Phys Rev Lett 79:237
147. Kim S, Misner M, Xu T, Kimura M, Russell T (2004) Adv Mater 16(3):226
148. Zhang Q, Tsui OKC, Du B, Zhang F, Tang T, He T (2000) Macromolecules 33(26):9561
149. Kim G, Libera M (1998) Macromolecules 31:2569
150. Turturro A, Gattiglia E, Vacca P, Viola GT (1995) Polymer 36:3987
151. Alexandridis P, Spontak RJ (1999) Curr Opin Colloid Interface Sci 4:130
152. Park S, Kim B, Xu J, Hofmann T, Ocko BM, Russell TP (2009) Macromolecules 42(4):1278
153. Xu T, Stevens J, Villa J, Goldbach JT, Guarini KW, Black CT, Hawker CJ, Russell TP (2003) Adv Funct Mater 13:698
154. To T, Wang H, Djurisic AB, Xie MH, Chan WK, Xie Z, Wu C, Tong SY (2004) Thin Solid Films 467:59
155. Huang H, Hu Z, Chen Y, Zhang F, Gong Y, He T, Wu C (2004) Macromolecules 37:6523
156. Harant AW, Bowman CN (2005) J Vac Sci Technol B 23:1615
157. Tokarev I, Krenek R, Burkov Y, Schmeisser D, Sidorenko A, Minko S, Stamm M (2005) Macromolecules 38:507
158. Tang Y, Lu JR, Lewis AL, Vick TA, Stratford PW (2002) Macromolecules 35(10):3955
159. Vogt BD, Soles CL, Jones RL, Wang CY, Lin EK, Wu Wl, Satija SK, Goldfarb DL, Angelopoulos M (2004) Langmuir 20(13):5285
160. Mukherjee M, Singh A, Daillant J, Menelle A, Cousin F (2007) Macromolecules 40(4):1073
161. Wang W, Troll K, Kaune G, Metwalli E, Ruderer M, Skrabania K, Laschewsky A, Roth SV, Papadakis CM, Müeller-Buschbaum P (2008) Macromolecules 41(9):3209
162. Vogt BD, Soles CL, Lee HJ, Lin EK, Wu W (2005) Polymer 46(5):1635
163. Olszowka V, Hund M, Kuntermann V, Scherdel S, Tsarkova L, Böker A (2009) ACS Nano 3(5):1091–1096

164. Olszowka V, Hund M, Kuntermann V, Scherdel S, Tsarkova L, Böker A, Krausch G (2006) Soft Matter 2:1089
165. Papadakis CM, Di Z, Posselt D, Smilgies DM (2008) Langmuir 24(24):13815
166. Tsarkova L (2010) Prog Colloid Polym Sci, in press
167. Helfand E, Tagami Y (1972) J Chem Phys 56(7):3592
168. Fredrickson GH, Leibler L (1989) Macromolecules 22(3):1238
169. Mondal MH, Mukherjee M, Kawashima K, Nishida K, Kanaya T (2009) Macromolecules 42(3):732
170. Barbero DR, Steiner U (2009) Phys Rev Lett 102(24):248303
171. Perlich J, Koerstgens V, Metwalli E, Schulz L, Georgii R, Müeller-Buschbaum P (2009) Macromolecules 42(1):337
172. Fredrickson GH, Bates FS (1996) Annu Rev Mater Sci 26:501
173. Koneripalli N, Levicky R, Bates FS (1996) Langmuir 12:6681
174. Lambooy P, Russell TP, Kellogg GJ, Mayers AM, Gallagher PD, Satija SK (1994) Phys Rev Lett 72:2899
175. Hamersky MW, Hillmyer MA, Tirrell M, Bates FS, Lodge TP, von Meerwall ED (1998) Macromolecules 31:5363
176. Yokoyama H, Kramer EJ (1998) Macromolecules 31:7871
177. Yokoyama H, Kramer EJ, Fredrickson GH (2000) Macromolecules 33:2249
178. Yokoyama H, Kramer EJ (2000) Macromolecules 33:954
179. Cavicchi KA, Lodge TP (2003) J Polym Sci B Polym Phys 41:715
180. Cavicchi KA, Lodge TP (2004) Macromolecules 37:6004
181. Harrison C, Adamson DH, Cheng Z, Sebastian JM, Sethuraman S, Huse DA, Register RA, Chaikin PM (2000) Science 290:1558
182. Harrison C, Cheng Z, Sethuraman S, Huse DA, Chaikin PM, Vega DA, Sebastian JM, Register RA, Adamson DH (2002) Phys Rev E 66:01170671
183. Müller M, Katsov K, Schick M (2003) J Polym Sci B 41(13):1441
184. Constantin D, Oswald P (2000) Phys Rev Lett 85(20):4297
185. Matsen MW (1998) J Chem Phys 110:4658
186. Ludwigs S, Krausch G, Magerle R, Zvelindovsky A, Sevink G (2005) Macromolecules 38(5):1859
187. Sevink GJA, Fraaije JGEM (2008) Macromolecules 1:53
188. Brinkmann S, Stadler R, Thomas EL (1998) Macromolecules 31(19):6566
189. Stadler R, Auschta C, Beckmann J, Krappe U, Voigt-Martin I, Leibler L (1995) Macromolecules 28(9):3080
190. Chen HY, Fredrickson GH (2002) J Chem Phys 116(3):1137
191. Chen P, Liang H (2006) J Phys Chem B 110(37):18212
192. Huang Y, Liu H, Hu Y (2006) Macromol Theory Simul 15(2):117
193. Fukunaga K, Elbs H, Krausch G (2000) Langmuir 16(7):3474
194. Kulbaba K, Manners I (2002) Polym News 27:43
195. Granick S et al (2003) J Polym Sci B 41:2755

http://www.springer.com/978-3-642-12875-2

Complex Macromolecular Systems I
Müller, A.H.E.; Schmidt, H.-W. (Eds.)
2010, XII, 220 p. 154 illus., Hardcover
ISBN: 978-3-642-12875-2